Block Copolymer Nanolithography for Sub-50 nm Structure Applications

Löfstrand, Anette

2021

Document Version:
Publisher's PDF, also known as Version of record

Block Copolymer Nanolithography for Sub-50 nm Structure Applications

ANETTE LÖFSTRAND
DEPARTMENT OF PHYSICS | FACULTY OF ENGINEERING | LUND UNIVERSITY

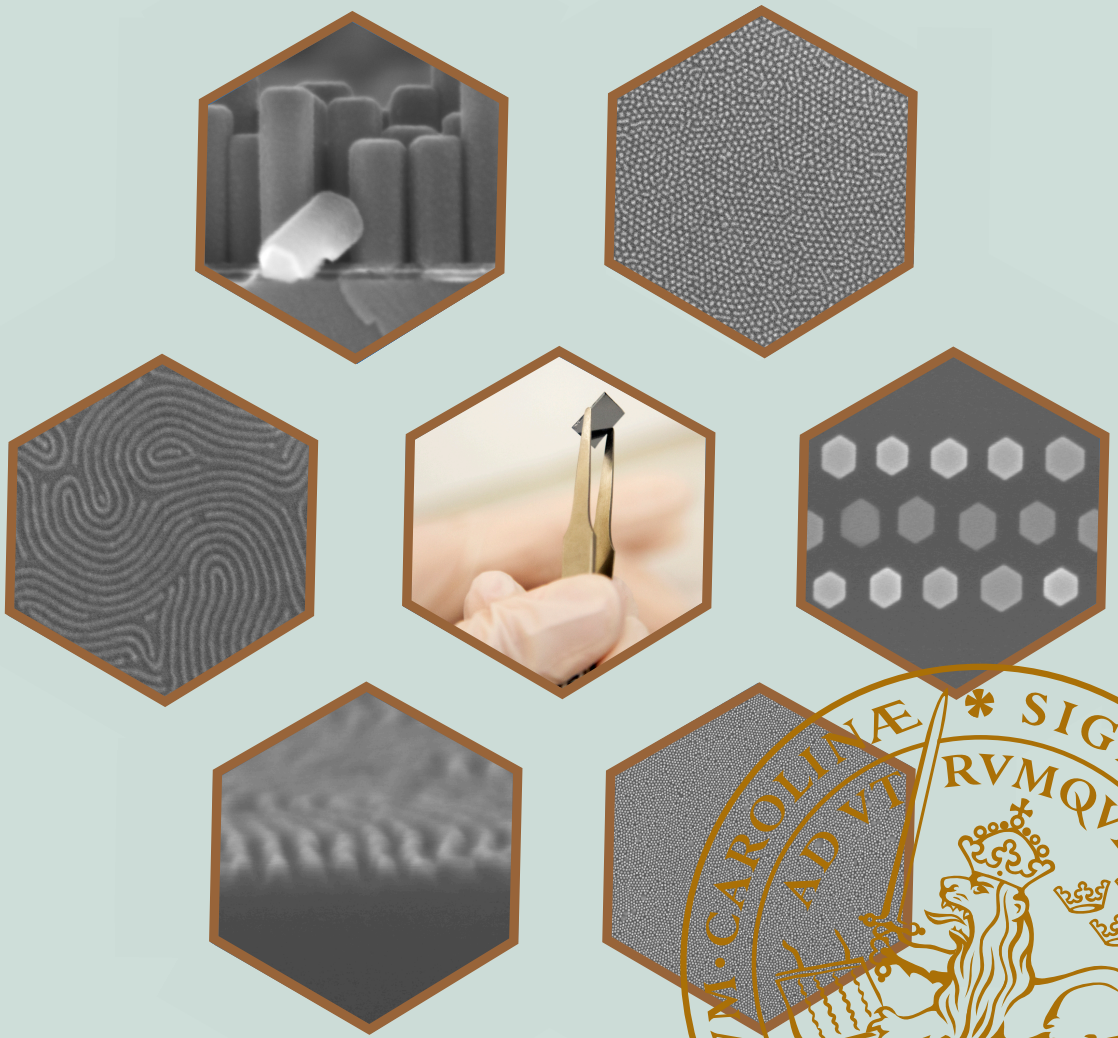

Block Copolymer Nanolithography for Sub-50 nm Structure Applications

Anette Löfstrand

LUND
UNIVERSITY

DOCTORAL DISSERTATION

by due permission of the Faculty of Engineering, Lund University, Sweden.
To be defended at Rydbergssalen, the Physics Department, Sölvegatan 14, Lund, on the 26th of November 2021 at 09.15.

Faculty opponent
Ass. Prof. Tamar Segal-Peretz
Technion - Israel Institute of Technology, Israel

Organization	Document name
LUND UNIVERSITY	DOCTORAL DISSERTATION
	Date of issue November 2, 2021
Author: Anette Löfstrand	Sponsoring organization

Title and subtitle: Block Copolymer Nanolithography for Sub-50 nm Structure Applications

Abstract

As high technology device patterns are continuing to move towards decreasing critical dimensions and increasing pattern density, there is a need for lithography to move in the same direction. Block copolymer (BCP) lithography is a promising technique, which has single digit nanometer resolution, has a pattern periodicity of about 7-200 nm, and easily scales up to large area at a low cost. The use of BCPs with high immiscibility of constituent blocks, so-called high-χ material, enables smaller pattern dimensions and is therefore of special interest. However, for lithography techniques to be applicable, also integration into existing nanofabrication processes is necessary. Furthermore, development of techniques to perform sub-10 nm pattern transfer is an enabler for continued device development. This dissertation first provides an overview of the BCP lithography field, to thereafter study the selective infiltration synthesis of alumina into the maltoheptaose block in high-χ poly(styrene)-*block*-maltoheptaose of 12 nm pattern periodicity. The infiltration was studied using neutron reflectometry, and a subsequent sub-10 nm pattern transfer was performed into silicon. Also, it studies the process of surface reconstruction of high-χ poly(styrene)-*block*-poly(4-vinylpyridine) of 50 nm pattern periodicity, more specifically the effect of time and temperature on pore diameter. Furthermore, pattern transfer of the surface reconstructed BCP film into silicon nitride, and selective area metal-organic vapor phase epitaxy (SA-MOVPE) of indium arsenide vertical nanowires on a silicon platform, using directed self-assembly is demonstrated. By directing the self-assembly along different crystal directions of the substrate, two vertical nanowire configurations were grown. Demonstration of gate all-around stack deposition of oxide/metal to the densely packed nanowire configurations was thereafter made. The results have contributed to the knowledge on BCP lithography and pattern transfer in the sub-50 nm regime, enabling new approaches for applications such as vertical nanowire, or fin transistors.

Key words: block copolymer, directed self-assembly, surface reconstruction, pattern transfer, sequential infiltration synthesis, neutron reflectometry

Classification system and/or index terms (if any)

Supplementary bibliographical information		**Language:** English
ISSN and key title		**ISBN** 978-91-8039-044-6 (print) 978-91-8039-043-9 (electronic)
Recipient's notes	**Number of pages:** 93	Price
	Security classification	

Signature 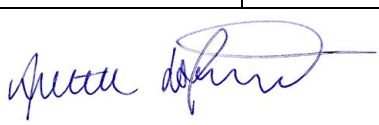 Date 2021-10-18

Block Copolymer Nanolithography for Sub-50 nm Structure Applications

Anette Löfstrand

LUND
UNIVERSITY

Cover photo (front): center piece photo by Charlotte Carlberg Bärg.
Surrounding images by Anette Löfstrand.

Cover photo (back): photo by Charlotte Carlberg Bärg.

978-91-8039-044-6 (print)
978-91-8039-043-9 (electronic)

Faculty of Engineering, Lund University, Sweden
Physics Department

Printed in Sweden by Media-Tryck, Lund University
Lund 2021

To my dearest family – Dan, Albin, and Edvin.

Table of Contents

Abstract

As high technology device patterns are continuing to move towards decreasing critical dimensions and increasing pattern density, there is a need for lithography to move in the same direction. Block copolymer (BCP) lithography is a promising technique, which has single digit nanometer resolution, has a pattern periodicity of about 7-200 nm, and easily scales up to large area at a low cost. The use of BCPs with high immiscibility of constituent blocks, so-called high-χ material, enables smaller pattern dimensions and is therefore of special interest. However, for lithography techniques to be applicable, also integration into existing nanofabrication processes is necessary. Furthermore, development of techniques to perform sub-10 nm pattern transfer is an enabler for continued device development. This dissertation first provides an overview of the BCP lithography field, to thereafter study the selective infiltration synthesis of alumina into the maltoheptaose block in high-χ poly(styrene)-*block*-maltoheptaose of 12 nm pattern periodicity. The infiltration was studied using neutron reflectometry, and a subsequent sub-10 nm pattern transfer was performed into silicon. Also, it studies the process of surface reconstruction of high-χ poly(styrene)-*block*-poly(4-vinylpyridine) of 50 nm pattern periodicity, more specifically the effect of time and temperature on pore diameter. Furthermore, pattern transfer of the surface reconstructed BCP film into silicon nitride, and selective area metal-organic vapor phase epitaxy (SA-MOVPE) of indium arsenide vertical nanowires on a silicon platform, using directed self-assembly is demonstrated. By directing the self-assembly along different crystal directions of the substrate, two vertical nanowire configurations were grown. Demonstration of gate all-around stack deposition of oxide/metal to the densely packed nanowire configurations was thereafter made. The results have contributed to the knowledge on BCP lithography and pattern transfer in the sub-50 nm regime, enabling new approaches for applications such as vertical nanowire, or fin transistors.

Popular Science Summary in Swedish

Vad kan vi göra för att vidareutveckla högteknologin, som vårt samhälle bygger på idag? Tillverkning av högteknologisk utrustning kräver ofta att mönster görs på nanometerskala, dvs i storleksordningen från miljondelar av en millimeter till knappt en tusendel av en millimeter. Detta arbete handlar om hur mönster ner till 5 nm kan göras genom att använda en särskild typ av polymer. Denna kallas för sampolymer och består av minst två olika delar, som inte vill sammanblandas. Generellt kan man säga att ju svårare delarna har att blandas, desto mindre strukturer kan man göra. Att göra mönster för att överföra dem till ett annat material kallas även för litografi med mönsteröverföring. Det finns alltså ett intresse från såväl industrin, som från universitet, att vidareutveckla litografi- och mönsteröverföringstekniker.

Arbetet visar dels hur man kan överföra linjer med endast 12 nm periodicitet ner i kisel, dels hur man kan göra en mall för att växa nanotrådar med endast 50 nm periodicitet, vilka båda skulle kunna användas för exempelvis vidareutveckling av transistortillverkning. Genom att belägga en yta med en tunn sampolymerfilm och sedan utsätta filmen för ångor från lösningsmedel, har polymeren först organiserats i olika mönster – med liggande eller stående cylindrar av den ena polymerdelen. Dessa mönster kan även styras, genom att polymeren läggs på en yta med vägledande linjer. Om man dessutom gör dessa linjer i samma riktning som ytans kristallriktning, alltså i samma riktning som atomerna ligger ordnade i materialet under, kan man få särskilt ordnade uppställningar av stående nanotrådar när man senare växer material från ytan.

Innan man kan växa material från ytan måste man på något sätt överföra mönstret. Ett sätt är att göra en mall, då man först öppnar upp porer i cylinderdelen av polymeren genom att sänka ner den i alkohol, och här har visats att framför allt en förhöjd alkoholtemperatur gav en större pordiameter, samt ett något glesare mönster. Då porerna öppnats har sedan s.k. torretsning använts för att öppna upp hålen hela vägen ner till ytan inunder. Torretsning utförs med hjälp av gaser i en lågtryckskammare, där endast vissa typer av material tas bort på ett välkontrollerat sätt. Därefter har materialet inunder etsats vid de blottlagda hålen, medan det skyddats av den kvarvarande polymeren runtomkring. För att sedan kunna växa nanotrådar användes substrat av kisel, belagda med halvledarmaterialet indiumarsenid, samt ett tunt lager kiselnitrid. Med hjälp av sampolymer, organiserad längs linjer i substratets kristallriktning, har porer öppnats upp och mönsteröverförts genom kiselnitriden. För att minimera skador på den känsliga ytan har den sista kiselnitriden i hålen etsats bort i syrabad. Därefter

lades substratet i en lågtryckskammare vid hög temperatur med ångor, där både indium och arsenik ingick. Från ytan kommer, under rätt förutsättningar, vertikala trådar av indiumarsenid att växa. Märk väl att de endast kommer att växa upp ur öppningarna i kiselnitriden. På grund av att materialet växer snabbare i vissa riktningar än andra, kommer nanotrådarna att få ett karakteristiskt sexkantigt utseende i genomskärning. Det har här visats att rader med 35 nm breda stående nanotrådar, med cirka 50 nm periodicitet, kunnat styras antingen till en ordnad uppställning, där mellanrummen mellan trådarna är mer triangulära, en s.k. stjärnkonfiguration, eller också till en, där mellanrummen är mer jämna, en s.k. solkonfiguration. Eftersom sådana nanotrådar kan användas för att göra transistorer, och intresset att få plats med fler transistorer per ytenhet aldrig verkar avta, har även oxid- och metallager lagts på för att demonstrera hur grind runtom (*eng. gate all-around*) ter sig för dessa tätt stående nanotrådar. Detta är nämligen ofta ett efterföljande steg för att göra transistorer.

Ett helt annat sätt att göra mönsteröverföring från sampolymerer är att infiltrera polymeren med ämnen som innehåller metall, respektive syre. Om detta görs i en lågtryckskammare vid förhöjd temperatur, kan de tillförda ämnena reagera med vissa funktionella grupper i polymeren, och sedan bilda metalloxid där. Detta kallas då för ett hybridmaterial. I arbetet har en sampolymer använts, som har sådana funktionella grupper endast i den ena delen av polymeren. På så vis har aluminiumoxid bildats i enbart cylinderdelen av mönstret, medan övrig polymer förblivit oförändrad. Härigenom underlättades mönsteröverföringen avsevärt, då hybridmaterialet kan motstå etsning mycket längre tid än polymeren. Det kvarvarande mönstret av hybridmaterial har här sedan använts som mall, för att överföra ett linjemönster med 12 nm periodicitet ner i kisel. Även denna typ av mönster skulle kunna vara användbart vid transistortillverkning, till exempel s.k. FinFET:ar, som ofta har höga fenor etsade i kisel. Utöver detta har infiltreringsgraden i polymerer undersökts med hjälp av s.k. neutronreflektometri. Då används en samlad stråle av neutroner, vilken reflekteras mot ytan. Varje typ av ämne reflekteras sedan på ett unikt sätt. Genom att titta på den reflekterade strålen kan man sedan bestämma vilka ämnen som ligger på ytan, samt hur tjocka de olika lagren är. Metoden har använts för att undersöka hur olika parametrar inverkar på infiltrationsgraden, där upp till 40 vol% aluminiumoxid uppnåtts i polymeren maltoheptaose, medan polystyren var opåverkad. Resultaten bidrar således till vidareutvecklingen av litografi med mönsteröverföring på nanometerskala, särskilt för strukturer mindre än 50 nm.

Acknowledgements

My deepest gratitude goes to my main supervisor *Ivan Maximov*, who always has been supportive, interested, and had time to listen to both optimistic ideas and less successful experimental outcomes, and never failed to help finding solutions. I am also very grateful for all the knowledge and support provided by my co-supervisor *Lars-Erik Wernersson*, who always managed to find something positive and encouraging to say, even at times when the goal seemed distant. He has made me feel very welcome also at EIT Nanoelectronics group meetings. I would also like to express my gratitude to *Johannes Svensson*, who has been highly involved in the projects regarding nanowire growth. A special thank you goes to *Bengt Meuller*, who took the time to build the solvent vapor annealing chamber for our projects.

Furthermore, I appreciate all my wonderful colleagues at Solid State Physics and NanoLund – room mates, lab staff, management, administrators, IT, fellow PhD students, postdocs, research engineers, technical staff, cleaning personnel, and others I regularly meet, who found the time for a chat about life in general, work, or about science. These chats have been providing both energy and new ideas into my work. All time spent in the lab would not have been the same without all the wonderful people at the Nanoelectronics group, EIT. Our discussions have been filled with equal parts everyday life and science, which both have pushed me forward. Thank you all!

I would like to extend my gratitude also to *Francesc Perez-Murano* and his group at IMB-CNM, who was kind enough to welcome me to their research facility in Barcelona in the spring of 2017, which progressed my understanding of block copolymer lithography, but perhaps equally important expanded my network in the research field. I would also like to thank all my collaborators around the world that I have had the pleasure to work with! Even at times when the scientific outcome differed from the expected one, we gained some new knowledge.

I would like to thank all students, course responsible persons, and collaborators from teaching, boards, various groups, and projects, whom I have had the pleasure to work with! There is always something to learn. One person can do great things, but together we can complement each other, and reach much further!

Without financial contributions my research would not have been possible. I thank GreeNanoFilms, Swedish Foundation for Strategic Research, Nanoscience Foundries

and Fine Analysis – Europe, Royal Physiographic Society of Lund, Super-ADAM, NanoLund, and MyFab for making my PhD studies possible.

I would also like to thank my family – especially my mother, father, brothers, husband, and sons – and all my friends, both close and more distant, for all support and understanding during my PhD studies. I especially apologize if I have been out of touch lately! Thank you all, from the bottom of my heart!

Abbreviations

3D	Three-dimensional
AFM	Atomic force microscope/microscopy
ALD	Atomic layer deposition
-b-	*-block-*
BCP	Block copolymer
DSA	Directed self-assembly
DMF	Dimethyl formamide
EBL	Electron beam lithography
EDS	Energy dispersive X-ray spectroscopy
FET	Field effect transistor
FTIR	Fourier transform infrared
GAA	Gate all-around
GIC	Graphite intercalation compound
GISANS	Grazing incidence small-angle angle neutron scattering
GISAXS	Grazing incidence small-angle angle X-ray scattering
HOPG	Highly oriented pyrolytic graphite
HSQ	Hydrogen silesquioxane
ICP	Inductively coupled plasma
ILL	Institute Laue-Langevin
IRDS	International roadmap for devices and systems
LER	Line edge roughness
MH	Maltoheptaose
MOVPE	Metal-organic vapor phase epitaxy

NIL	Nanoimprint lithography
NR	Neutron reflectometry
ODT	Order-disorder transition
P4VP	Poly(4-vinylpyridine)
PAA	Poly(acrylic acid)
PB	Poly(butadiene)
PDMS	Poly(dimethyl siloxane)
PDSS	Pentamethyl disilylstyrene
PEO	Poly(ethylene oxide)
PI	Poly(isoprene)
PLA	Poly(lactide)
PMMA	Poly(methylmethacrylate)
PS	Poly(styrene)
PS-OH	Hydroxyl-terminated poly(styrene)
PVBD	Poly(5-vinyl-1, 3-benzodixole)
QCM	Quartz crystal microbalance
RIE	Reactive ion etching
RF	Radio frequency
SA-MOVPE	Selective area metal-organic vapor phase epitaxy
SEM	Scanning electron microscope/microscopy
SERS	Surface enhanced Raman spectroscopy
SIS	Sequential infiltration synthesis
SLD	Scattering length density
STEM	Scanning transmission electron microscope/ microscopy
SVA	Solvent vapor annealing
TEM	Transmission electron microscope/microscopy
TMA	Trimethyl aluminium
TMIn	Trimethyl indium

UV	Ultraviolet
VLS	Vapor-liquid-solid
VNW	Vertical nanowire
VPI	Vapor phase infiltration
WZ	Wurtzite
ZB	Zincblende

List of Papers

The thesis includes the following papers, which are appended:

I. Poly(styrene)-*block*-Maltoheptaose Films for Sub-10 nm Pattern Transfer: Implications for Transistor Fabrication

Löfstrand, A., Jafari Jam, R., Mothander, K., Nylander, T., Mumtaz, M., Vorobiev, A., Chen, W.-C., Borsali, R., and Maximov, I.

ACS Appl. Nano Mater., 5141 (11pp), 2021.

Contributed to conceptualization evolution, and with investigation (of BCP self-assembly, SIS, pattern transfer, NR), writing original draft (especially BCP self-assembly, SIS, NR, conclusions), formal analysis (of data from ellipsometry, AFM, SEM, NR), validation, writing review and editing, visualization, and methodology (especially BCP self-assembly, SIS, NR).

II. Sequential Infiltration Synthesis into Maltoheptaose and Poly(styrene): Implications for sub-10 nm Pattern Transfer

Löfstrand, A., Vorobiev, A., Mumtaz, M., Borsali, R., and Maximov. I.

Manuscript, (13pp), 2021.

Contributed to conceptualization evolution, and with investigation (of SIS, NR), writing original draft, formal analysis (of data from ellipsometry, NR), validation, visualization, and methodology (SIS, NR).

III. Feature Size Control Using Surface Reconstruction Temperature in Block Copolymer Lithography for InAs Nanowire Growth

Löfstrand, A., Svensson, J., Wernersson, L.-E., and Maximov. I.

Nanotechnology, 31, 325303 (9pp), 2020.

Contributed with conceptualization formulation of size dependence on SR temperature, to conceptualization evolution, and with investigation (BCP self-assembly, SR temperature, pattern transfer, however, NW epitaxy in close

collaboration with J. S.), writing original draft, formal analysis (of data from ellipsometry, AFM, SEM), validation, writing review and editing, visualization, and methodology (especially BCP self-assembly, SR temperature, pattern transfer).

IV. Directed Self-Assembly for Dense Vertical III-V Nanowires on Si and Implications for Gate All-Around Deposition

Löfstrand, A., Jafari Jam, R., Svensson, J., Jönsson, A., Menon, H., Jacobsson, D., Wernersson, L.-E., and Maximov. I.

Manuscript, (20pp), 2021.

Contributed with conceptualization (SR, DSA, gate all-around oxide and metal deposition), to conceptualization evolution, and with investigation (BCP self-assembly, SR temperature, pattern transfer, gate all-around oxide and metal deposition, however, NW epitaxy in close collaboration with J. S.), writing original draft, formal analysis (of data from ellipsometry, AFM, SEM, TEM), validation, visualization, and methodology (especially BCP self-assembly, SR temperature, pattern transfer).

The following papers are out of scope of this thesis and are therefore not included:

Sequential infiltration synthesis and pattern transfer using 6 nm half-pitch carbohydrate-based fingerprint block copolymer

Löfstrand, A., Jafari Jam, R., Mumtaz, M., Mothander, K., Nylander, T., Vorobiev, A., Rahaman, A., Chen, W.-C., Borsali, R., and Maximov, I.

SPIE Advanced Lithography Proceedings, Advances in Patterning Materials and Processes XXXVIII, 116120W (9pp), 2021.

Design and Development of Nanoimprint-Enabled Structures for Molecular Motor Devices

Lindberg, F. W., Korten, T., Löfstrand, A., Rahman, M. A., Graczyk, M., Månsson, A., Linke, H., and Maximov, I.

Mater. Res. Express, 6, 025057 (9pp), 2019.

Nanoimprint Stamps with Ultra-High Resolution: Optimal Fabrication Techniques

Graczyk, M., Cattoni, A., Rosner, B., Seniutinas, G., Löfstrand, A., Kvennefors, A., Mailly, D., David, C., and Maximov, I.

Microelectronic Engineering 190, 73 (6pp), 2018.

1 Introduction

Society today is to a high extent built upon high technology devices, and these devices often require patterning, or lithography. Lithography is a term generally thought of as producing a topological pattern of a specific design in a material, often to enable subsequential processing. The term originates from the Greek words *lithos* for 'stone', and *graphein* for 'to write', and in 1796 a printing technique was invented where wax was used to draw on top of a flat stone, which then was further processed to selectively deposit ink for printing on paper [1]. Today, lithography for micro- and nanofabrication comprises of several different patterning techniques, and development within the area of lithography could help to improve efficiency and to lower cost in many application areas. The classical lithography techniques typically use charged particles or light to modify the exposed material, and selectively remove either the exposed or the unexposed material, but there are alternative techniques. First, looking at pros and cons of the more traditional patterning technique UV lithography, it is flexible in feature design, fast, enables large area patterning, and low cost for micron sized patterns. Extreme UV lithography uses 13.5 nm wavelength and can reach a 7 nm half-pitch resolution [2]. However, cost and stochastic defects increase rapidly as feature sizes decrease [3]. Another traditional patterning technique, electron beam lithography (EBL), is flexible in feature design, and has a lower feature size limit around 5 nm half-pitch, although isolated features can be as small as 2 nm [4], and even 3 nm pitch features have been shown by electron beam induced deposition [5]. However, the writing speed of a traditional EBL configuration is very slow, and the technique is therefore not suitable for large area patterning. Also, the so-called proximity effect, which broadens the exposure of features relative to their design, as well as the forward broadening, limits the minimum feature size made by EBL in dense patterns even further [6]. The proximity effect limits the minimum feature size also in a more advanced EBL configuration, in which you multiply the number of exposing electron beams. So, even though this configuration makes it a faster technique, it is therefore generally not suitable for very high-density patterns. A patterning technique alternative to exposing with light or charged particles is material self-assembly. Self-assembly of block copolymers is a good lithography candidate for highly dense sub-50 nm features. The resolution of block copolymer self-assembly is currently well within the single digit nanometer range, 3.2 nm half-pitch [7], and is considered to be a low-cost lithography method, especially since it has the ability to pattern very large areas. The self-assembly morphologies for diblock copolymers are somewhat limited, and the most oftenly used

pattern types from block copolymer lithography are cylinders in a hexagonal lattice, or lamellae, which both are suitable for a number of different application areas.

The origin of block copolymer (BCP) lithography is said to be a discovery by physicist P. M. Chaikin in the office of the polymer chemist L. J. Fetters in the late 1980s, where he in an electron micrograph noticed a hexagonal array of dots formed by a microphase separated BCP with 30 nm spacing [8]. Appreciating the length scale to be appropriate for some electron transport measurements, he then initiated research resulting in well-ordered spheres in monolayer poly(styrene)-*block*-poly(butadiene) (PS-*b*-PB) [9], removal of the PB block using ozone [10], and pattern transfer processes to achieve both polarities into silicon nitride [11]. Many research groups have followed in his footsteps and further developed the area of BCP lithography and nanofabrication.

For a BCP to be suitable for nanofabrication it should, in general, fulfil two requirements: (1) achieve a sufficient separation of the constituent polymer blocks, and (2) possibility to selectively modify a polymer block. The first requirement is mainly controlled by the immiscibility of the constituent blocks, where a high degree of immiscibility also is known as a high-χ material [12]. When a high-χ material is used it enables sharp transitions between phase-separated areas, and therefore a higher pattern resolution is possible. The second requirement becomes relevant for most cases of nanofabrication. By utilizing the dissimilarities in the constituent blocks, one of the blocks could be selectively removed [13, 14], selectively incorporated with inorganic material [15-17], or selectively swelled by solvents [18]. One technique to selectively form metal oxide inside one polymer block is to repeatedly diffuse molecules containing metal, and oxygen, respectively, into it, so-called sequential infiltration synthesis (SIS) [15]. By selectively swelling one block, pores can be opened in the BCP film, also known as surface reconstruction [19]. Furthermore, already in the polymer synthesis, one block could be made more electro-conductive [20], or be made to include other groups of interest. This selective modification can thereafter be exploited to enable pattern transfer into another material. There are also examples, where the BCP material is used in an application without pattern transfer e.g., organic/inorganic BCP electrolyte for battery applications [21], or BCP material for pH sensors [22].

1.1 Sequential Infiltration Synthesis and sub-10 nm Pattern Transfer

Although the resolution of self-assembled BCP can be well below 10 nm, it may be very challenging to selectively modify one of the constituent blocks, and to perform pattern transfer into another material at these feature sizes. Nanofabrication processes that are suitable for features in the order of hundreds of nanometers may be detrimental

for sub-10 nm features. Within the European project GreeNanoFilms [23] a 6 nm half-pitch carbo-hydrate based BCP was used [24]. Even if initial process development on blanket films looked very promising, the 6 nm half-pitch pattern transfer was not successful using polymer as etch mask. The first research question (RQ) of this work was:

RQ1: How to enable pattern transfer of the 6 nm half-pitch carbohydrate based BCP poly(styrene)-*block*-maltoheptaose (PS-*b*-MH)?

Researching RQ1 revealed challenges both in finding suitable characterization methods for these materials and at this scale, and in finding suitable etching tools. It turned out that the fabrication process answering RQ1 showed some limitations in possible aspect ratio after pattern transfer. Since the process utilized infiltration of alumina, to fabricate an etch mask, optimizing the degree of infiltration and the infiltration selectivity between constituent blocks was deemed relevant to enable enhancement of the aspect ratio after pattern transfer. Also, reducing material consumption was of interest. The second research question of this work was therefore:

RQ2: How do the process parameters in semi-static sequential infiltration synthesis of trimethyl aluminium and water into carbohydrate-based maltoheptaose (MH) and poly(styrene) (PS) influence the degree of infiltration?

Regarding applications, patterns consisting of tall fins at a small pitch, etched into silicon, could very well be used for next generation lateral field effect transistors (FinFETs) [25].

1.2 Pattern Transfer for Selective Area Nanowire Epitaxy

Scaling of transistors has been ongoing for decades. Moore's theory about future transistor development was presented in 1965 [26], but has an updated interpretation in the More Moore international roadmap for devices and systems (IRDS) [27]. For each generation, the cost per transistor should decrease, whereas the number of transistors per surface area should increase. Furthermore, should the power consumption be reduced. This aim to increase the number of transistors per surface area pushes development to move from two-dimensional transistor design to three-dimensional. By using cost-efficient BCP lithography at a high pattern density to template small footprint vertical nanowire transistors of III-V semiconductor material, suitable for low power consumption devices, and based on a silicon platform, all three points are addressed. The third research question was therefore:

RQ3: How to grow thin indium arsenide nanowires at a high pattern density templated by block copolymer lithography?

Researching RQ3 revealed challenges with contamination of the polymer mixture from containers and consumables, with deposition of material on indium arsenide in a hydrogen rich environment, and with surface damage sensitivity during epitaxy. Aiming to increase the yield, as well as the control, subsequent transistor processing should be facilitated, and a fourth research question was formulated:

RQ4: How will directed self-assembly (DSA) of block copolymer affect templated growth of indium arsenide nanowires, and the possibilities for gate all-around deposition?

These four research questions are all answered in the four papers that are included in this work.

1.3 Outline

In summary, the topic of this work is block copolymer nanolithography for sub-50 nm structure applications. Where the classical lithography approaches might fail in creating cost-effective solutions for dense features over large areas, BCP lithography has its greatest strengths. The work can be divided into two sub-topics: (1) sequential infiltration synthesis (SIS) and sub-10 nm pattern transfer, which is a hot topic for next generation lithography, and (2) nanofabrication using BCP templated pattern transfer for selective area nanowire epitaxy. Although the results could be used for several different applications, they could also be directly applied to the development of transistor fabrication.

Chapter 2 starts by describing BCPs, principles of BCP self-assembly, and then presents some self-assembly methods.

Chapter 3 is on the lithography step, presenting methods to selectively modify one of the constituent blocks.

Chapter 4 is dealing with the nanofabrication techniques pattern transfer, lift-off, electroplating, and nanowire growth.

Chapter 5 brings up several characterization methods suitable for BCP lithography, pattern transfer, and nanowires.

Chapter 6 is discussing some possible applications of BCP lithography, and BCP templated nanofabrication.

Chapter 7 presents results and discussion for each included paper.

Chapter 8 is containing some concluding remarks on challenges, limitations, and advantages regarding BCP lithography and nanofabrication, and finally

Chapter 9, which includes an outlook on suggestions for future work in the field.

2 Block Copolymer and Self-Assembly

This section will deal with the principles of block copolymer self-assembly, and how to direct the generated patterns.

2.1 Block Copolymer

Polymers are typically monomers in repeating units, linked into chains. A block copolymer consists of minimum two types of repeating units, each type repeating into a longer sequence, or block [28, 29]. The blocks are then covalently bonded together. Many different types of block copolymers exist. For lithography purposes, it is more common to work with diblock copolymers, which consist of two types of blocks. This configuration is of type A-B. It is, however, becoming increasingly more common to work with linear triblock copolymers, in configuration type A-B-A or A-B-C (see Figure 1). An advantage of the A-B-A configuration can be larger process windows to achieve self-assembly in the sub-10 nm regime, compared to an A-B configuration with the same domain spacing [30]. The A-B-C configuration can be an advantage when more advanced patterns, such as dot arrays inside lamellae, are desired [31, 32]. There are also other configurations, such as star-shaped block copolymer $(A\text{-}B)_n$ [33]. However, this work will focus exclusively on diblock copolymers, in the A-B configuration. An example of a commonly used A-B configuration copolymer is poly(styrene)-*block*-poly(methylmethacrylate) (PS-*b*-PMMA) (see **Figure 1**).

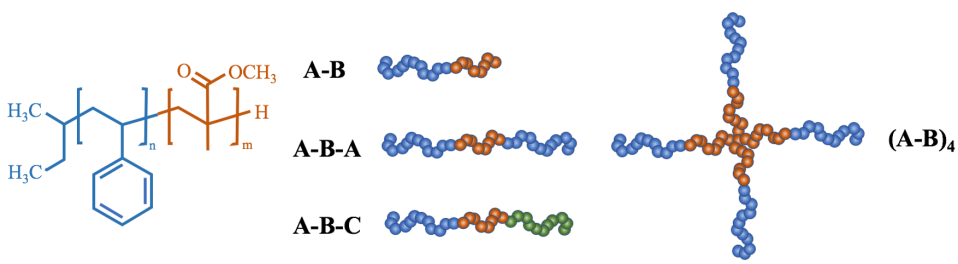

Figure 1. Block copolymer configuration schematic. To the left, PS-*b*-PMMA illustrating an example of an A-B configuration. To the right, diblock A-B, linear triblock A-B-A and A-B-C, and star shaped (A-B)n configuration.

Block copolymer synthesis was introduced by Szwarc in the 1950s, and was made by a so-called living polymerization of styrene and isoprene [34]. Living polymerization allows a high degree of control of compositions, molecular weights, and narrow molecular weight distribution, which are all important to achieve well-defined self-assembled BCP structures. Unless an end group is introduced to terminate the process, the polymer chain will continue to grow as long as there are available monomers for the reaction, and there are three general schemes used for the BCP synthesis: (1) if all monomer types A, B use the same reaction mechanism, addition of monomer B when A is consumed, (2) if the reaction mechanism of monomer A and B are incompatible, a functional end group can be introduced at the end of the A type chain, to thereafter add monomer B, or (3) addition of a functional end group to the end of the A type chain, as well as another functional end group to the end of the B type chain, to then let the two highly reactive functional end groups react to form the covalent bonds [28, 34]. The polymer poly(styrene)-*block*-maltoheptaose (PS-*b*-MH) used for sub-10 nm patterning in **Paper I** and **Paper II** was synthesized by the third synthesis scheme, using azido-functionalized (R-N_3) PS, propargyl-functionalized (HC≡C-CH_2-R') MH, and a copper catalyst in dimethyl formamide (DMF), and is described in detail in the supporting information of **Paper I**. The reaction utilizes the high reactivity of the triple bonds and is called click chemistry via copper-catalyzed azide-alkyne cycloaddition (see **Figure 2**). The molecular structure of the resulting BCP PS-*b*-MH is shown in **Figure 3**. After completion, the BCP is in powder form.

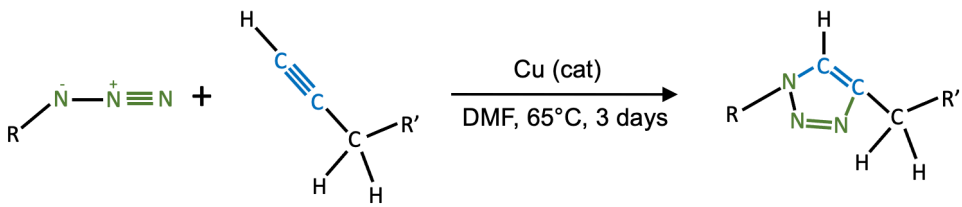

Figure 2. Reaction scheme for copper catalyzed azide-alkyne cycloaddition.

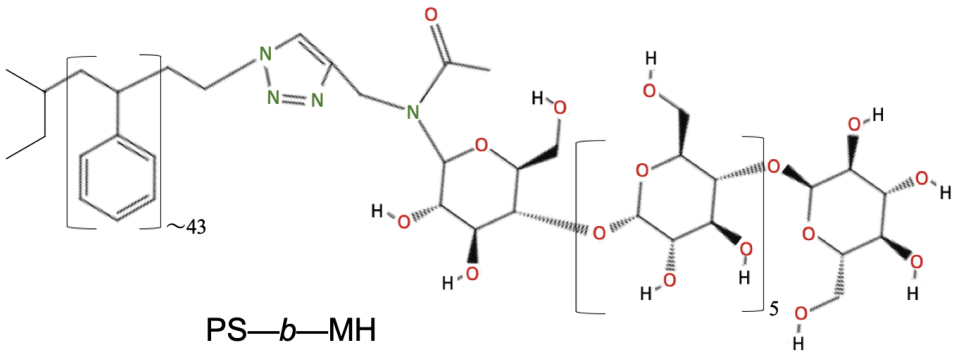

Figure 3. Molecular structure of poly(styrene)-*block*-maltoheptaose. Figure adapted with permission from [35], copyright 2021 the Authors. Published by American Chemical Society.

The BCP poly(styrene)-*block*-poly(4-vinylpyridine) (PS-*b*-P4VP) used for templating to grow nanowires at 50 nm pitch in **Paper III** and **Paper IV** was purchased readymade in powder form from Polymer Source Inc., Canada, and its molecular structure is shown in **Figure 4**. To be able to spin-coat the BCPs into thin films, the powder is dissolved in a solvent, and the weight percentage of BCP will then be the main factor controlling the film thickness.

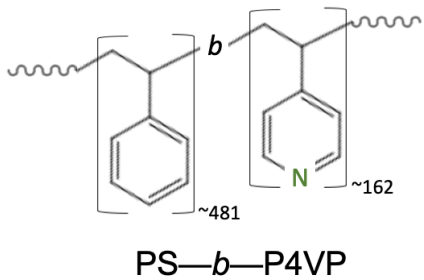

Figure 4. Molecular structure of poly(styrene)-*block*-poly(4-vinyl pyridine).

2.2 Self-Assembly

If the BCP blocks repel each other, and enough mobility is provided, they will micro-phase separate, much like oil and water phase separate. The blocks want to surround themselves with their likes, but as they are covalently bonded together, they will have to relate to one another (see **Figure 5**). This phenomenon can be utilized to generate

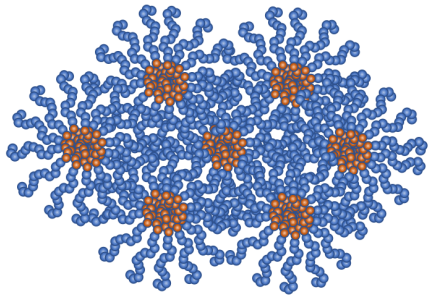

Figure 5. Diblock copolymer self-assembly into spheres/cylinders. 2D schematic.

micro-phase separated patterns for lithography purposes [36]. Block copolymer thermodynamics [12] describes the interaction between the blocks, how strongly they segregate, what shapes the blocks will form i.e., which morphology it will have, and what is required for segregation to occur. The polymer-polymer interaction is described by Flory-Huggins interaction parameter χ, where a high value represents immiscibility [28]. The Flory-Huggins interaction parameter χ for a diblock copolymer A-B is dependent on the temperature T according to

$$\chi \approx \alpha T^{-1} + \beta, \tag{1}$$

where $\alpha > 0$, and β is a constant for a given value of the volumetric block ratio f [12]. In other words, a lower temperature will favor phase segregation. Ordering of blocks may take place if the entropy is lowered by the ordering [12]. The degree of polymerization N is closely related to the polymer chain length [28]. The entropic contribution to the free energy scales as N^{-1}, whereas the enthalpic contribution scales as χ, and microphase separation takes place when the product χN is above approximately 10 [12]. At weak segregation, close to the transition from disorder to order, the pattern periodicity scales as $N^{1/2}$ [12]. If χN is much larger than 10 it is referred to as strong segregation, and here the pattern periodicity scales as $aN^{2/3}\chi^{1/6}$, where a is the characteristic block segment length [12]. Furthermore, the block-to-block interface width in strong segregation is narrow, and can be described by $a\chi^{-1/2}$ [12]. The interface width of PS-*b*-PMMA was found to be approximately 5 nm independent on molecular weight [37]. If the polymer chain length is too short, or the segregation is too weak, the diblock copolymer will not order into a self-assembled pattern. This puts a restriction onto the lower limit of pattern dimensions. A BCP of a high χ is thus necessary to enable sub-10 nm patterning [38]. Sinturel et al. scaled the effective Flory-Huggins interaction parameter χ_{eff} for various BCPs to a common statistical segment volume for comparison, and the χ_{eff} value for PS-*b*-PMMA was then 0.030, it was 0.40 for PS-*b*-P4VP, whereas it was 1.1 for poly(lactide)-*block*-poly(dimethyl siloxane) (PDMS-*b*-PLA) [38, 39].

The relative volume of the two blocks *f* in a diblock copolymer essentially determines the morphology of the BCP. In general, a relative volume A:B of 1:1 will give lamellae, whereas 1:4 will give a hexagonal lattice of cylinders of block A, inside a matrix of block B as can be seen in **Figure 6** [40]. These two morphologies are probably the most commonly used for lithography purposes. Furthermore, self-assembled spheres are occasionally used, and their assembly occur in the transition region from disordered to cylinder state [40]. More uncommon is the gyroid state, which occurs in the transition from cylinders to lamellae [40]. The equilibrium microphase separated pattern periodicity in the bulk is often referred to as domain spacing, or L_0. Typically, BCP work is being done on pattern periodicities of 10-50 nm, but up to 210 nm was reported using diblock copolymer PS-*b*-PMMA [41, 42], and down to 6.5 nm pattern periodicity

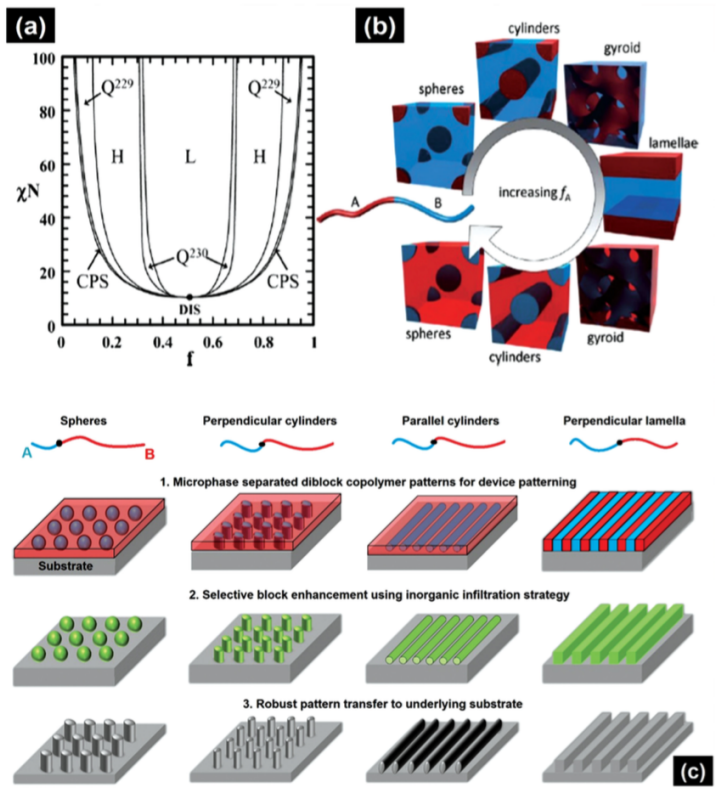

Figure 6. Microphase separation states of diblock copolymer. a) Typical theoretical binary phase diagram according to self-consistent field theory of diblock copolymers, where DIS denotes the disordered state, L lamellae, H hexagonal cylinders, CPS closely packed spheres, Q229 body centered spheres, Q230 double gyroids. Furthermore, χ denotes Flory-Huggins interaction parameter, N the overall degree of polymerization (related to the polymer chain length), and f the relative volume of the two blocks. **b**) Morphologies in a) illustrated, **c**) Corresponding lithography and pattern transfer scheme, using inorganic infiltration. Figure reprinted with permission from [16], copyright 2016 John Wiley and Sons; a) adapted with permission from [40], copyright 2006 American Chemical Society, and b) adapted with permission from [43], copyright 2010 Elsevier.

has been reported using special configuration type called three-armed cage BCP [7]. It can be noted, that it is also possible to use a combination of diblock copolymers A-B/B'-C purposing lithography of cylinders in a square lattice [44], a morphology which might be of interest for some applications.

Triblock copolymers in A-B-C configuration can self-assemble into morphologies, which are depending on the χN values of the interaction between respective polymer block [45]. Many interesting morphologies, such as square array dots, or dots arranged in separated lines can be induced (see **Figure 7**).

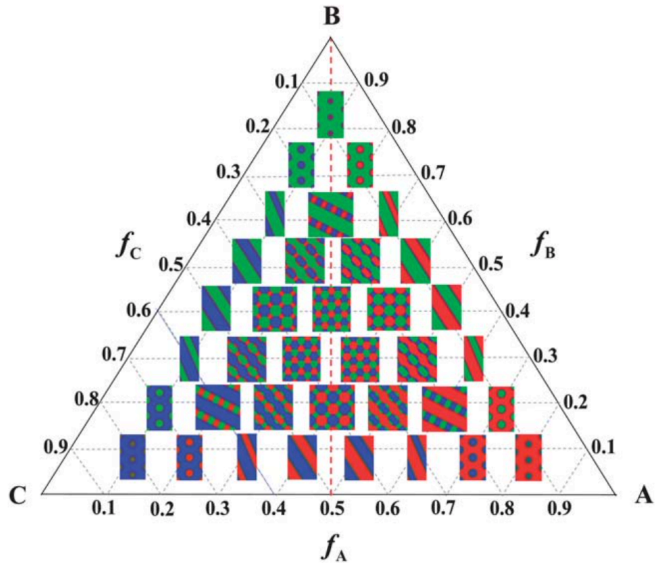

Figure 7. Ternary phase diagram of ABC star triblock copolymers in bulk. Structures are arranged in (f_A, f_B, f_C) for $\chi_{AB}N=\chi_{BC}N=\chi_{AC}N=40$. The red dashed line is the isopleth of the AC boundary. Figure reprinted with permission from [45], copyright 2013 The Royal Society of Chemistry.

2.3 Annealing

To self-assemble a BCP, a certain degree of polymer chain mobility is required. This can be achieved by adding either heat or solvent, a process which is called annealing. If the thermodynamic equilibrium state is represented by the desired morphology, an extended annealing time will result in an extended long range order [41], that is, the ordered pattern grain size will increase.

2.3.1 Thermal Annealing

By adding heat to the BCP, the polymer chains can get enough mobility to self-assemble into their most favorable state of energy. The temperature must be above the so-called glass transition temperature T_g, which is where the material starts to soften [28], and below, often just below, the order-disorder transition temperature T_{ODT}, where χN becomes too low for ordering to occur [46], but also preferably below the degradation temperature, where the material starts to deteriorate, although degradation could also affect self-assembly positively [47]. Thermal annealing [48] is often considered to be a more industrially adapted approach, as it is solvent free, and easy to integrate into a track. However, an increased temperature will also lower χ, according to **Equation 1**. After the thermal annealing has allowed the BCP to order, the BCP is quenched by quickly removing the sample from the elevated temperature to room temperature, and the morphology is frozen in its position. Thermal annealing of PS-*b*-PMMA has been shown to get less eccentric pores in vertical hexagonal cylinders for a film thickness in the same order as the pattern periodicity, a decreased pore diameter distribution with annealing time, and a decreasing pore size distribution and spacing distribution with increasing annealing temperature, up until 250°C, a temperature approaching the order-disorder transition temperature T_{ODT} [48].

2.3.2 Solvent Vapor Annealing

By annealing at room temperature, a high-χ can be maintained, according to **Equation 1**. Adding solvent to the BCP will disentangle the polymer chains, and increase the mobility, effectively lowering the glass transition temperature T_g of the polymer, enabling ordering at lower temperatures. In this case the polymer will swell, as solvent molecules will be penetrating the polymer [28]. When the solvent is introduced as vapor, the process is referred to as solvent vapor annealing (SVA). The so-called solubility parameter δ is commonly used to determine the solubility of substances, and can be given by the semi-empirically derived Hildebrand values, or by Hansen values, which includes van der Waal's dispersion forces, dipole-dipole interaction, and hydrogen bonding [28]. The difference between the Hansen solubility parameter of the polymer and that of the solvent should be less than approx. 2.5 $(MPa)^{1/2}$ to be soluble [49]. If two polymer blocks have very different solubility parameters, two solvents that selectively dissolve each block can be chosen. By using a mixture of these solvents, the relative volume of the two blocks can be altered, which can be used to tune the BCP morphology (see **Figure 6**) [50]. The ratio of solvents can not only control the type of morphology, but also the orientation of the pattern in a thin film [24, 50]. Solvent vapor annealing can thus be advantageous to enable vertical self-assembly in BCPs with a small pattern periodicity, suitable for subsequent lithography processing. A typical SVA duration lasts from a few minutes [51] to 24 h [52]. It has, however, been seen that BCP film dewetting might eventually occur after

longer solvent vapor annealing times, but by adjusting the substrate's surface energy, in relation to the desired BCP morphology, the dewetting can be suppressed [41]. Solvent vapor annealing, in a so-called jar, at room temperature was the technique used in **Paper I**, **Paper II**, **Paper III**, and **Paper IV**.

2.3.3 Solvothermal Annealing

A combination of adding heat and solvent to the BCP is used in microwave annealing [53, 54]. The processing time can then be reduced to the order of seconds, but the technique is still immature and, so far, only developed for smaller samples. Another so-called solvothermal annealing process, by first performing SVA, and subsequently adding a thermal quench, can reduce the annealing time substantially, in comparison to solely performing SVA [55]. The idea is then to not only control the swelling, but also the deswelling of the polymer, since both steps affect the final morphology of the BCP [55]. Another approach is to adjust the temperature during SVA [51]. By decreasing the temperature, the relative solvent vapor saturation increases, which in turn increases the polymer swelling [50], and control of the polymer swelling ratio is one way to effectively control the resulting BCP morphology [51].

2.3.4 Solvent Vapor Annealing Chamber

The classical method to perform SVA is to introduce liquid solvents into an enclosed container, where the sample is contact with the solvent in vapor form only, sometimes referred to as jar annealing (see **Figure 8**). An interest to increase the understanding of the process, as well as to find more industrial friendly solutions for SVA has led to further development [56], and has resulted in several different SVA chamber designs. One design uses the injection of liquid solvent into a chamber, but in combination with a controlled diluting nitrogen gas flow, and an in situ film thickness measurement tool, to control the degree of polymer swelling [57]. Another design uses so-called bubblers, where the solvent vapor is introduced via controlled flow of carrier gas though one or several solvent containers, along with a diluting nitrogen gas flow, and a film thickness measurement tool [50]. The bubblers can either contain one type of solvent, or a mixture of solvents. The design can be expanded to also include a heated stage [55, 58]. Addition of a computer-controlled heater with feedback from a film thickness measurement tool could further automate the SVA process [51].

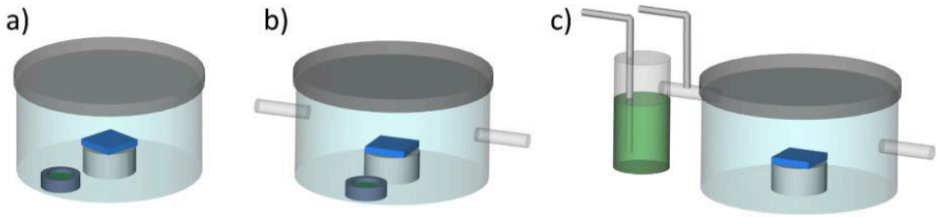

Figure 8. Schematic of solvent vapor annealing methods. a) jar annealing with sealed chamber containing the sample (blue), and the liquid solvent (green) reservoir, **b)** jar annealing with gas inlet and outlet, and **c)** solvent vapor flow via a carrier gas through inlet and outlet. Figure reprinted with permission from [56], copyright 2018 the Authors. Published by MDPI.

2.3.5 Solvent Evaporation Rate

Rapid quenching of a swelled BCP after SVA can lead to another morphology than slower deswelling would, and it has been suggested that a longer deswelling time will allow for relaxation into the thermodynamically favored morphologies [59]. However, the boundary conditions for the confinement where the polymer self-assembles will also change during the film deswelling [60], and a further elaboration on the topic can be found in **Chapter 2.4**. An example of SVA with slow deswelling is jar annealing with a small leak, allowed to anneal until all solvent has evaporated and the polymer has regained its original volume [61]. An experimental study on the effect of evaporation rate on BCP morphology showed propagation of morphology changes from the free surface towards the substrate for slower deswelling [59]. A simulation study, where evaporation was assumed to propagate from the free surface towards the substrate, showed a wider surface preference window for obtaining vertical cylinders in SVA than in thermal annealing, and that if the surface preference to the majority block was weak, or neutral, vertical cylinders would be promoted, whereas if the surface preference to the majority block was strong a fast solvent evaporation rate, and a strong solvent selectivity towards the majority block would be beneficial [62]. **Chapter 2.4** will describe surface preference further.

2.4 Bulk vs. Thin Films

When self-assembling a BCP thin film it will normally become a microphase separated continuous film (see **Figure 6**). The thermodynamics of disordered BCP bulk has no boundaries to consider. However, when moving to BCP thin films, which is most commonly used in BCP lithography, there are boundary conditions to take into account [60]. There will then be one interface between substrate and polymer, and another interface between polymer and air, or free space. As the self-assembly strives

for the most favorable state of energy, these interface energies become highly important. Modification of the surface energy of the substrate can be done in such a way that it is neutral to both blocks in a diblock copolymer, which means that both blocks are equally attracted, or it can be adjusted to attract only one of the two blocks [63]. This is also referred to as surface preference, wetting, or affinity to blocks. For lithographical purposes, neutral surface energies, or a slight affinity towards the majority block is often suitable, since it usually promotes vertical cylinder morphologies [63, 64]. One widely used method to create a substrate surface energy suitable for the intended BCP morphology, is using a so-called polymer brush layer. This brush polymer often contains a hydroxyl terminal group, that can bond to hydroxyl groups on e.g., a silicon surface, via a condensation reaction upon heating [64]. This method is called grafting, and the excess material can thereafter be removed in a solvent [65]. Another method of altering the substrate's surface energy is utilizing self-assembled monolayers, often of silanes [66].

Furthermore, the film thickness is relevant for the resulting morphology [63, 67, 68], as it defines the confinement between the substrate and free space, and the thickness is commonly presented as a factor of the polymer domain spacing L_0. Unless the thickness is optimized to the so-called commensurability condition, that is, fitting the self-assembled pattern into the confinement without introducing defects, resulting defects could be seen in form of mixed morphologies, larger holes, or islands in the BCP film [60, 68]. Self-assembly of BCP thin films were used in **Paper I**, **Paper II**, **Paper III**, and **Paper IV**.

2.5 Directed Self-Assembly

As BCP self-assembly is affected by the surface energy of the substrate, as well as by other restrictions to the polymer confinement, the self-assembled pattern can be directed by both substrate topography, and by local surface energy modification. This is known as directed self-assembly (DSA) [69-74]. Directing the pattern using substrate topography is referred to as grapho-epitaxy [75, 76], whereas directing using local surface modification is referred to as chemo-epitaxy [30, 65, 67, 77]. Guiding patterns are typically made by other lithographical techniques, such as EBL [78], or immersion lithography [79].

A grapho-epitaxial pattern can be made by creating a topography in one single material e.g., by etching a pre-defined pattern into a substrate, to thereafter remove the etch mask [80]. Another approach is to create the topography in several materials, such as a pre-patterned EBL resist, or an oxide, resting on top of a substrate, which can be left to direct the self-assembly [76]. The guiding pattern can then be used with a brush layer [76], partly with [81], or without a brush layer [80]. A chemo-epitaxial pattern is

typically made by either (1) chemically modifying selected parts of a brush layer, to then remove the protecting mask (see **Figure 9**) [78], or (2) by etching pre-defined patterns into a polymer mat, which is affine to one block, and thereafter remove the etch mask, and selectively graft a brush layer affine to the other block to the underlaying substrate [77]. Lane et al. directed a 10 nm pitch BCP by using a nanoimprint lithography (NIL) defined guiding pattern in hybrid chemo-/grapho-epitaxy [82]. Pre-patterned EBL resist resting on top of a substrate was used for hybrid chemo-/grapho-epitaxial DSA without brush layer in **Paper IV**.

DSA can be used for the purpose of pattern densification [78, 79], pattern rectification (see **Figure 9**) [78], via hole shrinkage [83], as well as for extending the long-range order [67], or for control of pattern placement. It is also possible to use a BCP pattern to direct e.g., nanomaterial deposition [84].

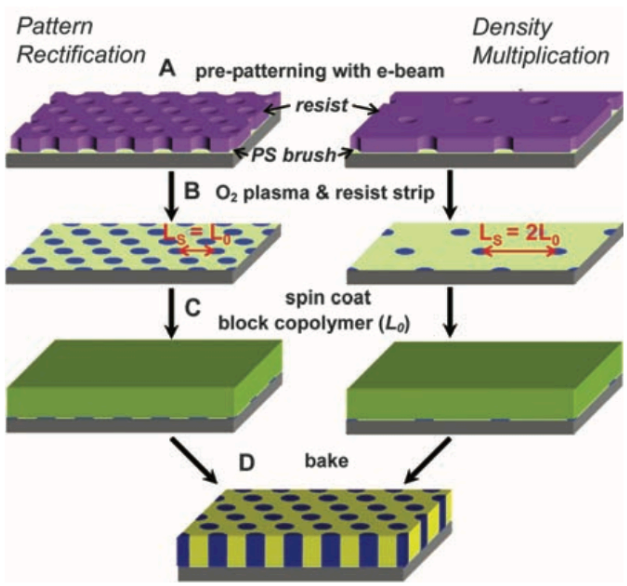

Figure 9. Schematic of process for DSA of BCP cylinders by chemo-epitaxy. A) Guiding patterns created using EBL, **B)** chemical activation of EBL-defined areas using O_2-plasma for stronger affinity to one block, **C)** deposition of BCP film, and **D)** DSA of the BCP to the underlying chemical pattern during annealing. From [78]. Reprinted with permission from AAAS.

In DSA, the BCP pattern defect level is strongly dependent on the lateral confinement size (see **Figure 10**) [67, 80]. The self-assembly can however adjust somewhat to different conditions. For example, the lamellae pattern periodicity of PS-*b*-PMMA directed by a chemo-epitaxial line pattern has been found to be able to stretch up to 2.5%, or compress up to 4.9% from the equilibrium bulk domain spacing L_0, without introducing defects [85].

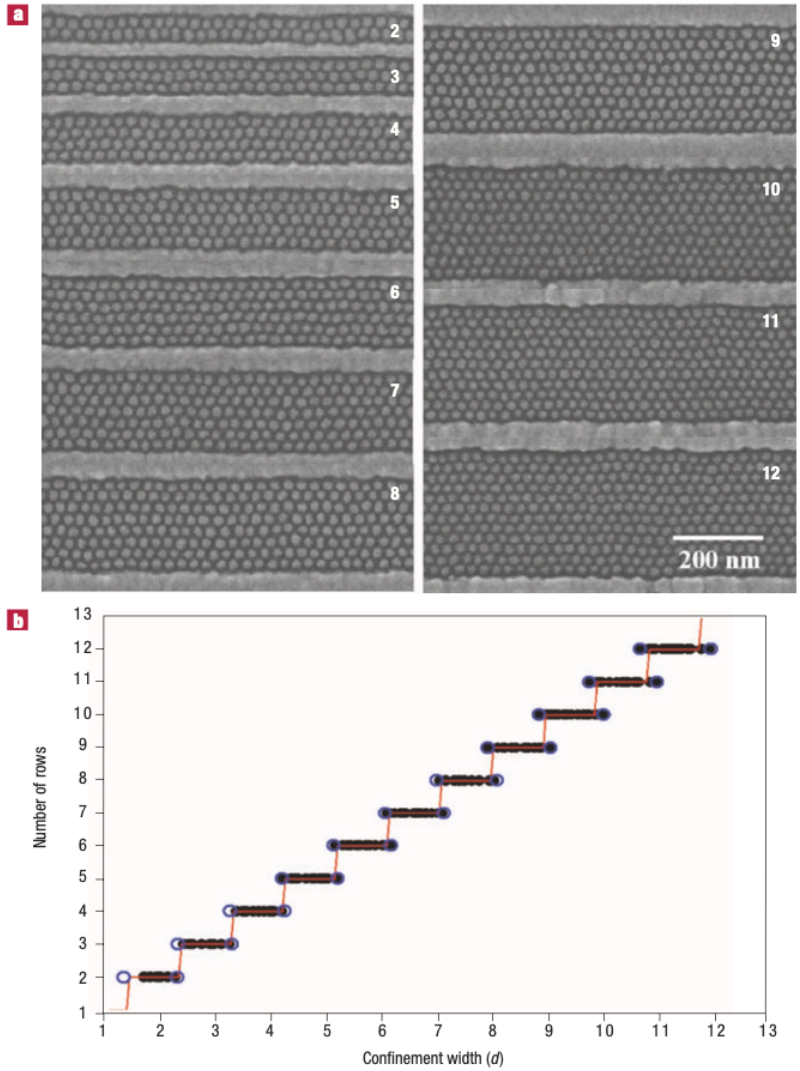

Figure 10. Directed self-assembly of BCP poly(styrene)-*block*-poly(ferrocenyl dimethylsilasane) by graphoepitaxy. a) showing SEM top view images of self-assembly by lines of different gap sizes, and **b**) showing the overlap of number of BCP rows fitted into a confinement. Figure adapted with permission from [80], copyright 2004 Nature Publishing Group.

It can be noted, that morphology alignment can also be performed by shear, building upon differences in mechanical properties of the blocks [86], zone annealing, which has a translational temperature gradient [87], zone casting, where BCP is deposited onto a slowly moving substrate [88], using electric fields, based on the differences in dielectric permittivity of the blocks [89], or magnetic fields, relying on anisotropy in the

magnetic susceptibility of the self-assembled BCP [90]. However, these techniques are not commonly used for BCP lithography purposes.

3 Block Copolymer Lithography

Block copolymer lithography can be used to produce patterns of several design types (see **Chapter 2.2**), but linear or hexagonal pattern designs are used for most applications. A general feature of BCP lithography is that the patterns are both high-resolution and high-density. The self-assembled BCP pattern consists of a microphase separated polymer layer, and therefore needs to be further processed to achieve the desired topology. This can be done if one of the polymer blocks is modified to be more easily removed than the other block. The technique is sometimes referred to as BCP lithography with a sacrificial component [91]. This is in analogy with classical lithography, where the material is modified by exposure to light or electrons to have a different solubility than the unexposed areas. Thereafter, the development is made by dissolving part of the polymer film [92]. In BCP lithography, there are numerous possibilities of achieving contrast e.g., by selective swelling and quenching of one block to open pores [93], by UV exposure modification and wet etching [94], by optimizing dry etching selectivity between blocks [95], by selectively infiltrating metal oxide into one block [15], or by selective inclusion of metal [96], and these techniques will be further presented in this chapter.

3.1 Surface Reconstruction

When Sohn et al. performed so-called surface reconstruction of a free-standing film of PS-*b*-P4VP in ethanol, i.e., without support of a substrate, it was shown to invert from having features of P4VP cores in a PS matrix, into features having PS cores in a P4VP matrix [97]. Some areas did, however, obtain a more donut-like shape of PS, and they also found indications that one block was wetting the entire surface [97]. When a polymer is exposed to a solvent within solubility range [49], it will swell, and its mobility will increase [28]. If a diblock copolymer spin-coated onto a substrate is exposed to a solvent, which is within solubility range of only one of the two blocks, typically the minority block, this block will swell. As long as the temperature is below the glass transition temperature T_g of the majority block [28], the majority block matrix will remain kinetically trapped in a glassy state, i.e., remain frozen [91]. The swollen minority block will no longer fit into the confinement defined by the majority block, and it will start to wet the polymer surface [19]. Upon drying, the minority block will collapse on

the majority block matrix [19]. This will allow the creation of pores as the film is quenched, quickly dried via solvent evaporation [18]. If the majority block remains frozen, the ordering of the BCP should be kept intact [98]. The technique is known as surface reconstruction, confined swelling-induced pore generation, or pore opening (see **Figure 11**) [19], and have been explored on BCPs, such as poly(styrene)-*block*-poly(acrylic acid) [99], PS-*b*-PMMA [18, 100], PS-*b*-P2VP, and PS-*b*-P4VP [93, 101-104]. The surface reconstruction has been found to be reversible upon heating above T_g, which could be explained by the kinetically entrapped BCP having a large surface area of the more hydrophilic block, having a higher surface energy [98]. Surface reconstruction has also been found to be, at least partly, reversible by using a solvent within the solubility range of the majority block [97]. Furthermore, immersion of a PS-*b*-P2VP film on a substrate into diluted HCl resulted in donut-shaped P2VP when the pattern periodicity was larger, but a continuous film of P2VP on top of the PS matrix when the periodicity was smaller [105]. Patterns of both vertical cylinders in a hexagonal lattice, and perpendicular lamellae have been successfully surface reconstructed [106]. Surface reconstruction of PS-*b*-P4VP has been used in **Paper III**, and **Paper IV**.

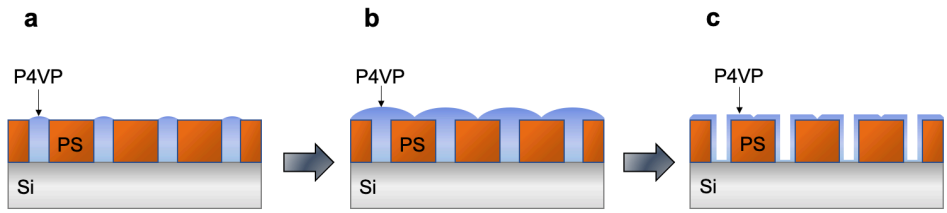

Figure 11. Schematic illustration of pore opening via surface reconstruction. **a**) Block copolymer self-assembled onto a substrate, **b**) swollen minority block after immersion into a minority block selective solvent, and **c**) open pores in the BCP film after solvent evaporation.

After surface reconstruction, the BCP can be used e.g., as a membrane [93], in a metal inclusion process [61], or for other subsequential processing to enable pattern transfer [102]. It should be noted that the process of surface reconstruction does not necessarily include any sacrificial component.

3.2 Etch Selectivity Between Blocks

A more classical approach to BCP lithography is to use photosensitivity. One example is modification of polymer blocks through UV exposure, which has been studied on e.g., PS-*b*-PMMA films [94]. A suitable UV exposure dose may predominately cross-link PS chains, making the PS more difficult to dissolve, whereas the same exposure

dose will break bonds in the PMMA chains, which will not only make the PMMA easier to dissolve, but also possible to remove from the BCP film using acetic acid; under condition that the chain scission occurs close to the block junction [94]. Also, other wavelength ranges may be used to modify polymer material e.g., 532 nm laser light has been used for ablation of polymer, i.e., when material is removed by photon irradiation, and it was found that both P2VP and poly(hydroxy styrene) were removed at higher rates than PS [14].

More common is use of dry etch selectivity between blocks in BCP, i.e., when one block is removed faster than the other in RIE. For example, features in PS-*b*-PMMA have been found to have an etch selectivity of 2:1 for PMMA over PS in RIE using Ar/O_2 plasma [95]. Another example is the use of N_2/H_2 plasma RIE of P2VP, P4VP, and PS, where an etch selectivity of 0.9:2:1 for the respective materials were found [13]. Since the difference between P2VP and P4VP is the position of nitrogen in the aromatic ring, the steric hindrance was believed to contribute to their etch selectivity [13]. Lane et al. were able to selectively remove poly(5-vinyl-1, 3-benzodixole) (PVBD) over pentamethyl disilylstyrene (PDSS) in CO_2 plasma RIE, and these polymers can form 10 nm pitch patterns as a diblock copolymer [82]. However, when the pattern periodicity is small, the interface region between the two blocks becomes proportionally large, and removal of the sacrificial component becomes more challenging [37]. This is an important area of research, since enabling high fidelity pattern transfer of sub-10 nm pitch could potentially have a great impact on manufacturing strategies of high technology devices. If the etch selectivity between blocks is too low, a common strategy is to incorporate inorganic material into one of the blocks, thereby increasing the etch selectivity.

3.3 Sequential Infiltration Synthesis

In atomic layer deposition (ALD), two precursors, often one metal-organic and one oxygen containing, are used in cycles to deposit a metal oxide in monolayers on top of a surface [107]. However, the same tool and precursors can be used to infiltrate a polymer with metal oxide, effectively creating a hybrid material; under the condition it is containing the necessary functional groups for reaction to occur, e.g., hydroxyl (-OH) [108], or carbonyl (>C=O) [109]. This process is also conducted in cycles of consecutive precursor exposures of each type, and the process is often referred to as vapor phase infiltration (VPI), or sequential infiltration synthesis (SIS) [15]. To achieve an increased contrast in a BCP, the metal oxide formation should occur selectively in only one of the blocks. The reaction between metal-organic precursor and functional group will then either be a reversible complex formation, or an irreversible chemical reaction [110].

Several factors regarding reaction mechanisms, thermodynamics, and kinetics should be taken into account in SIS: (1) available functional groups for precursor reaction [111], (2) solubility of precursor in the material, (3) diffusivity of precursor in the material [110], (4) effect of morphology on diffusion [112], (5) precursor partial pressure, (6) energy profiles for reaction pathways [108], and (7) forward and backward reaction rates [113]. Some amount of overlap does, however, exist between these points.

A well-studied SIS process is the use of trimethyl aluminium (TMA) and water precursors in PS-*b*-PMMA [114]. Under appropriate conditions, the precursors can diffuse into both blocks, and the TMA will react with carbonyl groups in the PMMA, whereas the PS is left unreacted. Dandley et al. found that during the initial exposure of the strong Lewis acid TMA it may form a reversible Lewis adduct with the carbonyl group in PMMA, that at lower temperatures the TMA can desorb, and that at higher temperatures a covalent bond can be formed [115]. Furthermore, they proposed that the reaction was yielding a covalent bond between Al-$(CH_3)_2$ and the oxygen from the previous carbonyl group (C=O), and the remaining methyl group (-CH_3) from TMA reacts with the methoxy group (-O-CH_3) in PMMA. During the subsequential water exposure, water will supposedly adsorb to the methyl groups, react to form a covalent bond between the hydroxyl group from water and an aluminium atom, and at the same time form the by-product methane (CH_4) [116], similar to the reaction occurring in the ALD case [107].

These reactions led to creation of alumina inside the PMMA block (see **Figure 12**). The metal oxide feature dimensions of an infiltrated BCP are known to increase with number of infiltration cycles [114]. Also, titanium oxide has been reported to have been SIS incorporated into PMMA using $TiCl_4$ and water precursors [114]. By using an initial pulse of TMA to create a nucleation site, infiltration of other materials are also possible, such as zinc oxide, or tungsten [109]. Other examples of polymers known to have been successfully infiltrated with TMA and water are P2VP [113], P4VP [117], polyisoprene (PI) [118], poly(acrylic acid) PAA, and poly(vinylpyrrolidone) [119].

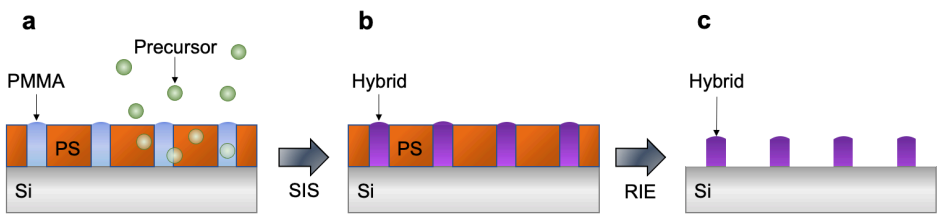

Figure 12. Schematic illustration of sequential infiltration synthesis. a) Cyclic infiltration of precursors into the self-assembled BCP, **b**) selective formation of metal oxide inside one of the blocks resulting in a hybrid material, and **c**) remaining hybrid material after removal of unaltered polymer block in RIE.

SIS using TMA and water into PS-*b*-MH, hydroxyl-terminated PS (PS-OH) and MH was investigated in **Paper I**, and in the latter two materials in **Paper II**. By using e.g., oxygen plasma RIE the unaffected polymer can be removed, effectively leaving a hybrid material pattern on the substrate, and this RIE process has also been found to be effective for sub-10 nm patterns [30]. The hybrid pattern could later be used as an etch mask, which was the strategy used in **Paper I**.

3.4 Selective Metal Inclusion

Surface reconstruction can be utilized to incorporate metal into the opened pores, using e.g., a metal salt [96], or metal nanoparticles [106]. Cho et al. showed that by spin-coating a solution of gold salt $HAuCl_4$ in ethanol onto a surface reconstructed PS-*b*-P2VP film, and then exposing it to heat, or toluene vapor, the gold-loaded P2VP was drawn into the pores [104]. They found that the size of the gold particle was related to the concentration of gold salt in the solution. Furthermore, both iron salt $FeCl_3$ and titanium isopropoxide could be used in the same manner [104]. Another method to include gold, is to immerse a PS-*b*-P2VP film on a substrate into a solution of $HAuCl_4$ and diluted HCl, thereafter rinse, dry, and use oxygen plasma to remove the polymer and reduce the metal salt to Au(0) [105, 120]. Furthermore, by including silver acetate in a PS-*b*-P4VP solution prior to spin-coating, silver salt could be selectively located in the P4VP block, and the silver salt could even be inverted, together with the P4VP, during surface reconstruction of a free-standing film [97]. In the particle case, palladium particles in an aqueous solution have been found to interact preferentially with the P4VP block of PS-*b*-P4VP, using capillary forces and affinity to one of the blocks to deposit material selectively [106].

Park et al. has found that when evaporating a very thin layer of gold onto a surface reconstructed film of PS-*b*-P4VP and thereafter heating it moderately, the gold will diffuse, preferentially interact with the P4VP block, and coalesce to form nanoparticles [98]. Using a slightly thicker gold layer in combination with a higher temperature resulted in a ring-like pattern, since some of the gold then was remaining on the majority block regions [98]. The various metal inclusion techniques provide the possibility of a high dry etch selectivity between metal and polymer, which e.g., can be done in oxygen plasma RIE. The metal patterns can be then be used e.g., as an etch mask for pattern transfer [103], or as catalysts [91].

4 Nanofabrication

The term nanofabrication could be considered to include all the processing steps, from BCP synthesis, via annealing, to subsequent processing. However, in this chapter, the subsequent fabrication steps which are applicable to also be used in combination with other lithography techniques are collected. One cornerstone in nanofabrication is transfer of the lithographically defined pattern into the underlying substrate. It can e.g., be transferred into a hard material for further processing. Integration of BCP lithography into existing processes may sometimes be challenging but is an important part of research within the field.

4.1 Pattern Transfer

In pattern transfer, etch selectivity between materials is utilized, i.e., that one material can be removed at a higher rate than another material [121]. Openings can then be defined in the material with the lower etch rate, to protect selected areas of the material underneath. A more classical example is using a UV-sensitive polymer, i.e, a UV-resist, on top of a silicon substrate, UV-expose selected areas of the polymer, to thereafter dissolve the exposed parts of the polymer to make openings in the polymeric film [122]. This film can also be used as an etch mask. By dipping the substrate into a suitable wet etchant, the substrate material can be removed at a much higher rate than the protective polymer material [121]. After etching, the polymeric film can be removed, and the pattern from the etch mask has been transferred into the underlying material. This process is known as pattern transfer. Many wet etchants etch isotropically, i.e., at the same etch rate in all directions, and one example is wet etching of silicon in HF/HNO_3 [123]. Isotropic etching limits the possible aspect ratios in the pattern transfer. Other wet etchants etch anisotropically, at different etch rates in different crystal directions e.g., wet etching of crystalline silicon in KOH [124, 125].

The most common way to perform pattern transfer at the nanometer scale today is probably by reactive ion etching (RIE), which can be made to etch anisotropically [92, 126]. Reactive ion etching is performed in a low-pressure chamber, where gases are introduced, selected to have a low etch rate of the mask, and a high etch rate of the

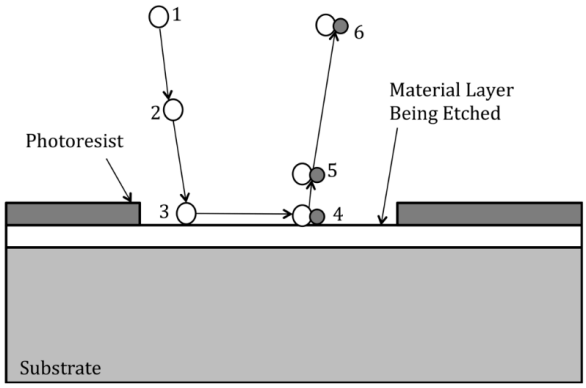

Figure 13. Schematic of the chemical part of reactive ion etching. 1) Process gases ionized into chemically reactive species in plasma, **2**) reactive species moving towards substrate, **3**) reactive species adsorbing to the surface, **4**) diffusion and reaction between reactive species and material layer, **5**) volatile reaction compound desorbing, and **6**) volatile compound diffusion. Figure reprinted with permission from [126], copyright 2021 the Author. Published by MDPI.

material to be structured. Inside the chamber, one electrode, i.e., the sample stage, is connected to a radio frequency (RF) power source via a capacitor, and another electrode is connected to ground [92]. Free electrons will then be accelerated by the generated electric field, collide with the gas molecules and ionize them, converting the molecules to reactive species [92]. Some of the ions and electrons will recombine and emit light, which causes the typical plasma glow [92]. The electrons move faster than the ions, and the electrode connected to the RF power source will create a self-biased electric field, accelerating the ions toward it, and toward the substrate placed on it [92]. There will be one physical, and one chemical component of the RIE [92]. After adsorbing to the substrate surface, the reactive species may diffuse along the substrate, and react with material at the substrate's surface. (see **Figure 13**) [126]. The formed volatile compounds can thereafter desorb and diffuse away from the substrate. The chamber is continuously pumped, why the compounds will be removed. The described process is the chemical component of RIE and gives a more isotropic etch. As most chemical processes, the etch rate will increase with temperature [92]. The physical component of RIE is ion sputtering, where the ions transfer their energy to atoms in the solid material, and these atoms may therefore escape [92]. This sputtering process has almost no lateral etching and therefore gives a more anisotropic etch [92]. In an inductively coupled plasma (ICP) RIE, the plasma can be generated and sustained by a separate RF electromagnetic field, which can increase the plasma density, thus the amount of reactive species, at low pressures [126]. The use of a separate RF field for plasma generation makes it possible to minimize the sputtering effect of having a high RF field at the sample stage [92]. A low chamber pressure further increases the anisotropic etching since fewer collisions then occur on the ion's pathway. Thus,

etching in ICP-RIE can be controlled by selection of etching gases and their flows, ICP RF power, temperature, sample stage RF power, and chamber pressure [92].

One example of material etch selectivity in RIE, is silicon nitride which normally etches faster than polymer using fluorocarbon based plasma chemistry [127]. Therefore, a BCP lithography defined polymer template can serve as an etch mask to transfer the pattern into the underlying silicon nitride. As BCP patterns typically have a high pattern density, highly anisotropic etching is to be preferred – the etching should be faster in the vertical direction. In **Paper I** ICP-RIE of silicon using BCP as an etch mask was performed, whereas in **Paper III** and **Paper IV** ICP-RIE of silicon nitride was performed with a BCP etch mask.

A slightly different approach to improve etch selectivity is to first perform pattern transfer into a thin layer of a so-called hard mask, i.e., a non-polymeric material later serving as an etch mask. The processing gases for the final pattern transfer and the hard mask material is then selected so that the hard mask material has a much lower etch rate than the material to be structured. An example of etching into a hard mask is 10 nm pitch pattern transfer from BCP into chromium [82].

Another way to improve etch selectivity in ICP-RIE is to lower the temperature in so-called cryo-etching [128], e.g., enabling an etch selectivity of silicon over polymer to be 10:1 in SF_6/O_2 plasma at a sample temperature of -120°C [129]. At such low temperatures the volatility of the by-products are reduced, but the vertical ion bombardment will sustain the etching in the vertical direction [128]. The addition of oxygen to the mixture also allows a thin passivating layer of SiO_xF_y to form on the side walls of the structure during etching, which further improves the etch anisotropy, and high aspect ratio features can be made also at the high pattern densities BCPs offer [129].

4.2 Lift-Off

By first performing BCP lithography with removal of a sacrificial component, an evaporation mask can be formed. A thin metal layer can thereafter be evaporated at a few degrees angle of incidence. The evaporation mask can then be lifted off in wet chemistry. An example is use of a PS-*b*-PMMA template of 30-35 nm structure height after mask completion, evaporation of 15 nm chromium at 5° angle of incidence, and lift-off in piranha [130]. The resulting metal nanostructures could e.g., be used as etch mask or for catalyst in epitaxy.

4.3 Electroplating

In electroplating, or electroforming, a current is flowing between two electrodes in an electrolyte, including metal cations e.g., Ni^{2+}. The conductive sample is mounted on the cathode, the negative electrode, which is connected to a power supply, and the metal cations migrate to the cathode. The cations are reduced to atoms, and deposit on the surface. If the surface is structured, a metal structure can be formed [131]. One example of application, is use of gold dot arrays as catalyst in epitaxy [132]. It should, however, be noted that a self-assembled BCP film has been reported to have been electroplated in $HAuCl_4/LiClO_4$ inside the poly(ethylene oxide) PEO domain, without sacrificial component removal [133].

4.4 Selective Area Metal-Organic Vapor Phase Epitaxy

Growth of material utilizing reaction and assembly of precursor gases is known as one of the bottom-up techniques. A commonly used technique to grow vertical nanowires is to let metal-organic vapors super-saturate a catalytic liquid gold droplet on top of a crystalline semiconductor surface, that promotes adsorption and growth as a solid at the interface of the semiconductor surface, the so called vapor-liquid-solid (VLS) technique [134, 135]. One advantage of vertical nanowire growth, is that it allows for a larger crystal lattice mismatch between the substrate and the grown material [135]. Another technique to grow material is selective area metal-organic vapor phase epitaxy (SA-MOVPE) [136]. It uses openings in an amorphous template down to a crystalline material (see **Figure 14**) [137]. It is of importance that the amorphous template film can tolerate the high temperatures used for selective area growth, and that the template etching method minimizes damage to the crystalline surface underneath [136]. The nucleation process of III-Vs inside the high temperature, low pressure chamber may be disrupted by the native oxide formed on the crystalline surface [138]. Just before

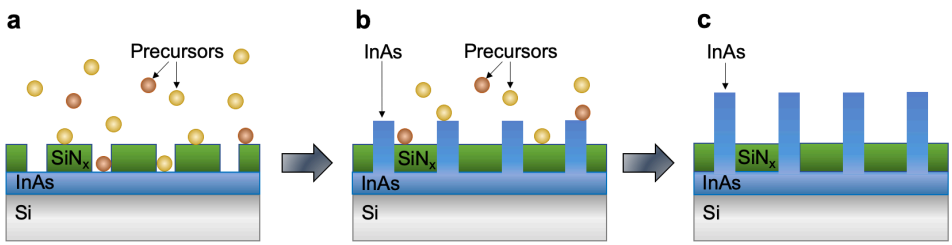

Figure 14. Metal-organic vapor phase epitaxy (MOVPE) schematic. a) A crystalline silicon (111) wafer, with an indium arsenide layer, covered with a template in amorphous silicon nitride. A flow of III-V precursors of arsine and trimethyl indium are introduced in a high temperature and low-pressure chamber. **b**) Indium arsenide nanowires grow preferentially in the <111>B direction, bottom-up, and **c**) resulting vertical InAs nanowires.

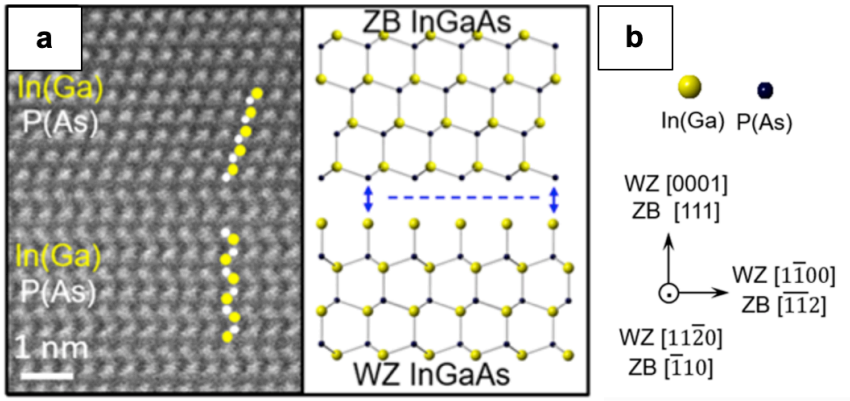

Figure 15. a) Aberration corrected scanning transmission electron microscopy (STEM) image taken along [$\bar{1}$10] or [11$\bar{2}$0] zone axis of zincblende (ZB) and wurtzite (WZ) regions, and illustration of corresponding atomic structures, and **b**) zone axes and color representation of atoms in illustration. Figure adapted with permission from [139], copyright 2018 American Chemical Society.

loading the sample into the MOVPE chamber, the indium arsenide native oxide (InO_x/AsO_x) should therefore be removed, which can be done in wet chemistry using e.g., HF or HCl [140]. A thermal cleaning process is usually also performed inside the MOVPE chamber prior to growth [138].

Selective area growth allows for more abrupt transitions between grown dissimilar materials than VLS growth does [141], which could be beneficial for nanowire heterostructure devices [142]. However, selective area growth usually has a higher density of transitions between the two crystal structure types zincblende (ZB) and wurtzite (WZ) (see **Figure 15**) [143]. Furthermore, both the nanowire diameter, and the nanowire length, is directly related to the size of the opening in the amorphous template – a smaller opening size will give a thinner and longer nanowire [136, 137]. A III-V material that is very promising for high performance devices [144, 145] is indium arsenide (InAs) due to its high electron mobility [138]. Indium arsenide grows preferentially in the <111>B crystal direction [146], and should therefore be grown on (111)B substrates, having group V atoms topmost, to get vertical nanowires. Vertical InAs nanowires therefore normally will get the characteristic hexagonal shape, having <110> facets (see **Figure 16**) [136].

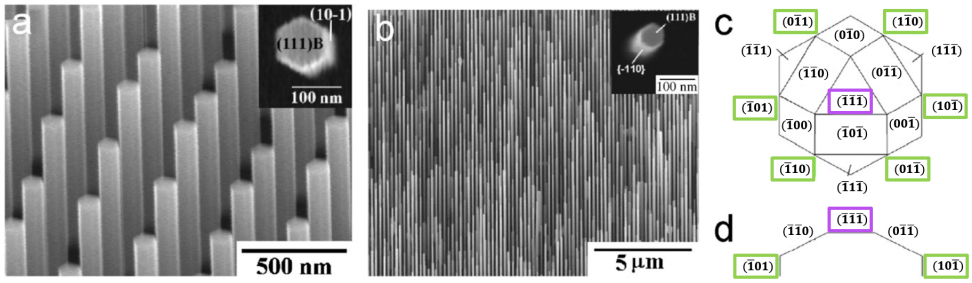

Figure 16. Selective area grown vertical InAs nanowires. **a**) and **b**) scanning electron microscopy images of nanowire arrays at 45° view angle, where insets are top views of single nanowires, **c**) top view diagram of low index planes around (111)B, and **d**) diagram of low index planes around (111)B in cross-sectional view. In diagrams, the vertical facets are marked with green, and the horizontal facets marked with magenta. Adapted from [137], copyright 2006, with permission from Elsevier, https://www.sciencedirect.com/journal/journal-of-crystal-growth.

BCP lithography has previously been reported to template selective area epitaxy of quantum dots [147-150], and of InAs nanowires from a gallium arsenide substrate with up to 32% nanowire yield (see **Figure 17**) [151], all using PS-*b*-PMMA. Selective area MOVPE from a BCP lithographically defined silicon nitride template has been used in **Paper III** and **Paper IV**.

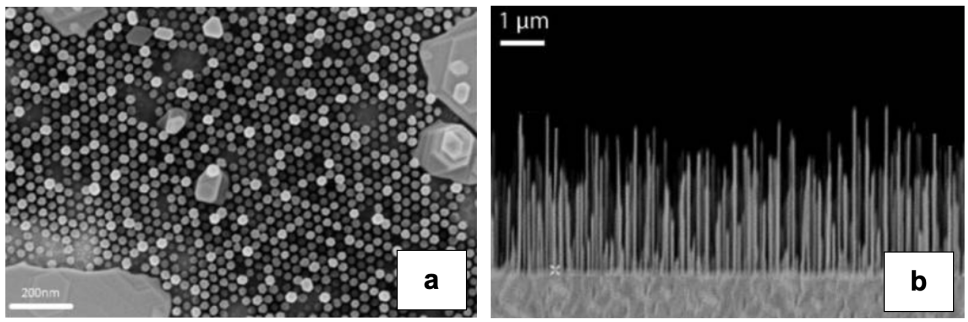

Figure 17. SEM images of InAs nanowires grown from a III-V substrate using a BCP lithography defined template. **a**) top view, and **b**) cross-sectional view. Figure adapted with permission from [151], copyright 2013 American Chemical Society.

5 Characterization

In nanotechnology, there is an obvious need of characterization tools, as the order of scale is beyond what the human eye can resolve from reflected light. Characterization of BCPs, and of nanofabricated samples made from BCPs, can be performed in many ways, depending on what type of information one is interested in. Spin-coated thin BCP films on top of substrates can be measured using ellipsometry [152, 153], to get information on film thickness and refractive index over a wavelength band (see **Figure 18**). By using in-situ optical spectroscopy, such as an ellipsometer, during solvent vapor annealing, information of the BCP film thickness, and thus the BCP swelling can be retrieved [50, 152]. In-situ investigation during SIS can provide information on precursor swelling and changes in refractive index [154]. Ex-situ ellipsometry has been used in **Paper I**, **Paper II**, **Paper III**, and **Paper IV**.

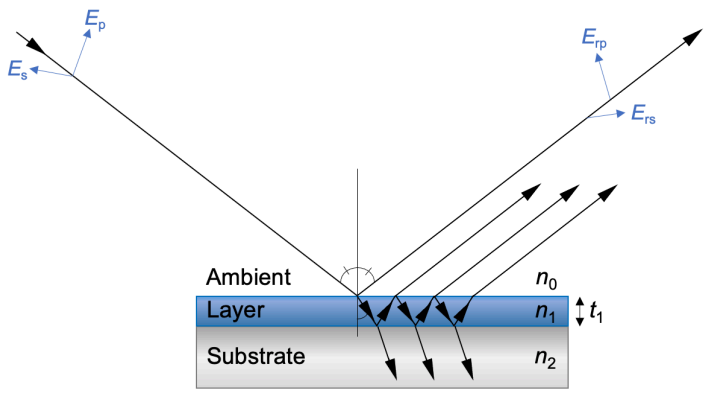

Figure 18. Schematic principle of ellipsometry. Incident polarized light of perpendicular components E_p parallel to the reflection plane and E_s orthogonal to the reflection plane. The components of the light reflected in the first interface is the reflected parallel E_{rp}, and the now phase shifted reflected orthogonal E_{rs}. The light may be reflected and transmitted at each material interface, and the sum of all reflected components can be detected. A model including the refractive indices n_0, n_1, n_2, and the layer thickness t_1 is thereafter fitted to the measurement.

Other in-situ characterization techniques suitable for SIS are quartz crystal microbalance (QCM), where mass gain can be analyzed, and Fourier transform infrared (FTIR) spectroscopy, where absorption peaks are used to analyze which molecular groups are contributing to the reactions [155].

Optical microscope bright field inspection can provide easily accessible information on the commensurability of the BCP self-assembly to the film thickness, as it is often possible to detect formation of larger islands or holes [60]. An atomic force microscope (AFM) can provide 3D information on surface topography, but also on material stiffness, which makes it possible to inspect a self-assembled BCP film even directly after self-assembly [156, 157]. Some polymers, such as PS and PMMA, can provide enough contrast to be resolved in a standard scanning electron microscope (SEM) [158], whereas others, such as PS and P4VP can be more difficult to resolve. However, after performing BCP pore opening of PS-*b*-P4VP, the topography can be inspected in SEM using a lower acceleration voltage [13]. In **Paper I**, **Paper II**, and **Paper III** AFM and SEM were used. Furthermore, energy dispersive X-ray spectroscopy (EDS) can be used to identify constituent elements and their concentrations in the analyzed area [158], although the lateral resolution is limited. In **Paper IV** EDS was used. It is also possible to use transmission electron microscopy (TEM) [157] for inspection of BCPs, but the preparation may be challenging. Polymers are often soft material, not prone to be easily cleaved at room temperature, and may also be damaged by the inspection itself. One way to prepare a self-assembled BCP film for TEM inspection is to lift it from a silicon substrate by immersion into HF solution, to thereafter place it on a TEM grid [98]. Another method to lift a BCP film is to spin-coat a BCP layer onto a mica substrate, to thereafter let it float off by immersion in water, driven by the strong affinity of water to mica [97]. Yet another approach, is to lift the BCP by having a layer of a water-soluble polymer such as PAA underneath, to thereafter let it float off in water [159]. After such a BCP layer transfer to a TEM grid, also scanning transmission electron microscopy (STEM) tomography can be used for three-dimensional view of BCPs [159]. For enhanced contrast in TEM, one of the blocks can be modified, and e.g., the P4VP block is known to have been selectively stained with I_2 vapor [97]. In **Paper IV** TEM and STEM of nanowires were used.

Perhaps less accessible techniques, grazing incidence small-angle X-ray scattering (GISAXS) and grazing incidence small-angle neutron scattering (GISANS) [160], can provide information on e.g., the self-assembly grain size, the periodicity, and the feature sizes available in the sample, measured and averaged over a micron range length scale. Also, neutron reflectometry experiments [161, 162] can provide information regarding e.g., the material depth profile. Since each isotope has as an associated ability to scatter neutrons, a so-called scattering length density (SLD) [163], information on constituent elements in the layers can be extracted. One example of such an instrument is the Super-ADAM reflectometer at Institute Laue-Langevin (ILL), Grenoble, France (see **Figure 19**) [164, 165]. This tool works at a single wavelength and scans the angle to get information in reciprocal space [165]. The neutron beam is led towards the instrument via highly oriented pyrolytic graphite (HOPG) and graphite intercalation compound (GIC) monochromators, providing neutrons having a wavelength λ of 5.2 Å [164]. Next to the monochromator, between collimation slits also known as diaphragms, is a

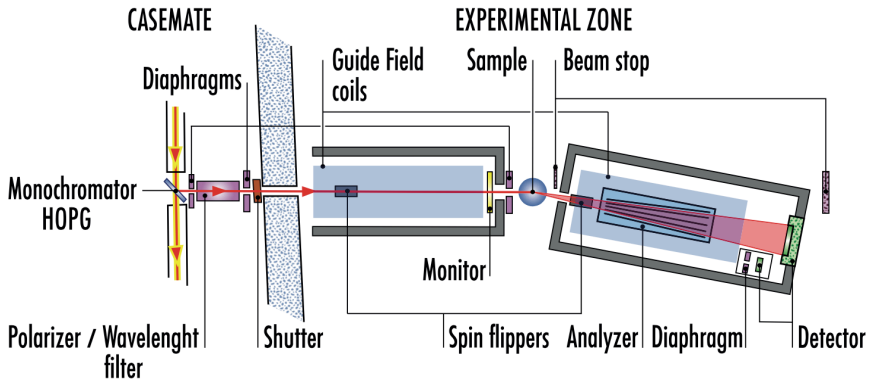

Figure 19. Schematic of the Super-ADAM neutron reflectometer layout. The tool is located at Institute Laue-Langevin, Grenoble, France. Reprinted from [165], with the permission from AIP Publishing.

solid-state filter suppressing wavelength harmonics, and optionally also polarizing the beam [164, 165]. Another slit is positioned before the sample. The incident beam angle can be controlled by a high-precision motorized sample stage, and the detector arm can be rotated around the sample. The distance between sample and detector is variable from 0.5 m to 6 m, and a position sensitive detector is used. Furthermore, various sample environments are possible [165]. Soft matter is often investigated using non-polarized specular neutron reflectivity, which is a grazing incidence technique [166]. The incident angle can then be swept, whereas the detection occurs at an outgoing angle, which is set to be the same as incident beam angle. The reflectivity R is the ratio of reflected beam and incident beam intensity [166]. Incident beam intensity can be measured using a monitor before the sample, or by measuring the direct beam [166]. The incident angle θ can then be related to the component of momentum transfer that is normal to the interface Q_z according to

$$Q_z = \frac{4\pi}{\lambda} sin\theta, \tag{2}$$

and typically, the reflectivity R is plotted versus Q_z, and a model of the sample layers, their SLD, thickness, and roughness is then fitted to the measured data, resulting in a SLD profile (see **Figure 20**) [166]. Specular neutron reflectometry was used in **Paper I** and **Paper II**.

Furthermore, the nanofabrication might result in a device, suitable for e.g., electrical measurements [167], or optical measurements [168, 169]. As a general note, it is highly valuable to be able to perform inspection after as many of the processing steps as possible, preferably without damaging the sample.

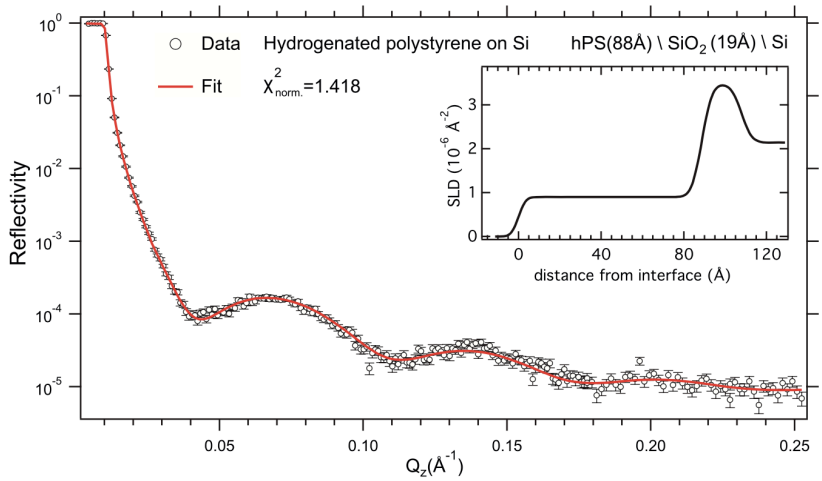

Figure 20. Experimental neutron reflectivity curve of a hydrogenated PS film on top of a silicon substrate along with the fitted model. Inset shows the scattering length density (SLD) profile of the fitted model. Reprinted from [165], with the permission from AIP Publishing.

6 Applications

Block copolymer lithography can be used for several application areas, and many of them involve highly dense dot or line patterns at sub-50 nm pitch. Dense dot patterns are used in e.g., surface enhanced Raman spectroscopy (SERS) bio- or chemical sensors [170], and bit pattern media [171]. Possible emerging application areas are III-V epitaxy templates for devices [138]. Examples of areas for vertical nanowire device applications are radial heterostructures for logic and memory, axial heterojunction for logic and sensing, photodetectors and light-emitting diodes, lasers, photovoltaics, photoelectrochemistry and photocatalysis, and thermoelectrics [142]. One high performance vertical transistor example is tunnelling FET (see **Figure 21**) [145, 172]. **Paper III** and **Paper IV** are focusing on processing techniques for vertical nanowire applications.

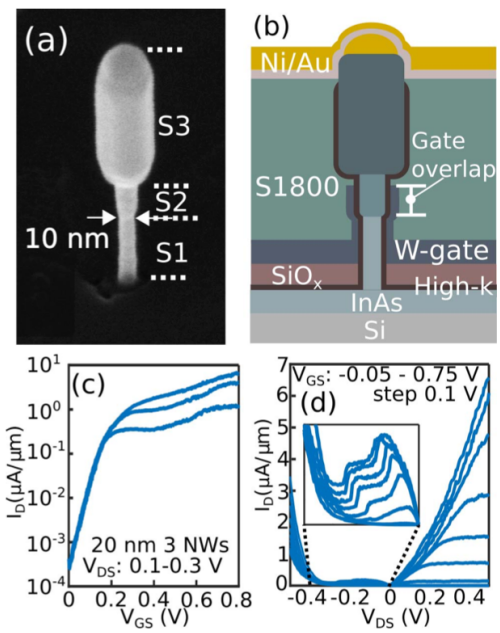

Figure 21. Vertical nanowire tunneling FET. **a**) Tilted view SEM image of 10 nm diameter nanowire device, where S1 is InAs, S2 is InGaAsSb, and S3 is GaSb, **b**) schematic of device, **c**) transfer data from 20 nm diameter device, and **d**) output data from 20 nm diameter device with inset from negative differential resistance region. The current is normalized to circumefrence and number of nanowires. Figure reprinted with permission [172], copyright 2018 IEEE.

Examples of dense line pattern applications are polarizing metal nanowire grids [173], organic FET memories, which were demonstrated using PS-*b*-MH [174], nanowire based chemical sensors [175], and organic photovoltaic devices [176]. A larger BCP pattern periodicity, of around 200 nm, enables optical applications in the visible range [177]. Furthermore, miniaturization, or rectification, of prepatterned surfaces, as in shrinking of via holes [83], rectification of EBL defined pattern [78], and sub 5 nm ultra-shallow junctions have been identified as potential routes for BCP lithography [178]. An example of a device from pattern densification via directed self-assembly (DSA) is 7 nm FinFETs (see **Figure 22**) [25]. **Paper I** and **Paper II** focuses on processing techniques applicable for e.g., lateral fin formation.

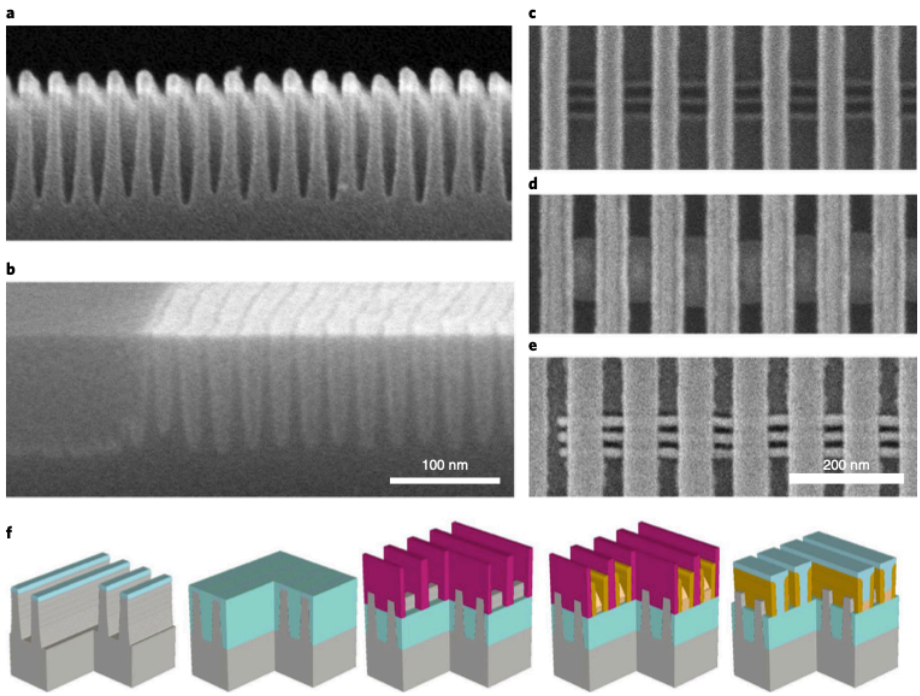

Figure 22. Stages of FinFET formation. Cross-sectional SEM images with same scale bar of **a**) fins etched into silicon using DSA, and **b**) fins filled with isolation oxide. Topview SEM images with same scale bar of **c**) dummy gate formation, **d**) source/drain merge, and **e**) dummy gate removal and channel exposure. **f**) schematic of structures in corresponding steps a) to e). Reprinted by permission from the Authors; Springer Nature Limited [25], copyright 2018.

A more general use of BCP lithography is for nanoimprint lithography master stamps [179], to enable swift replications of the generated pattern. If BCP layers are lifted from the substrate, they can also be used as pH-responsive membranes [93], for virus filtration [180], or for other types of filtering membranes [181]. Use of self-

assembled BCP as gate dielectric for organic thin film transistors has been reported [182]. Applications suitable from BCP lithography are including, but not limited to, the areas mentioned in this chapter. The firstmost requirement is an available BCP morphology to achieve the desired pattern. Second, integration of BCP lithography into subsequent fabrication is necessary. Third, an assessment of the maximum defect level for the application in question, and evaluation of the possibilities BCP lithography can offer. Apart from that, one of the limiting factors for possible applications is imagination.

7 Results and Discussion

In this chapter, the background, results, implications, and concluding remarks of the four included papers are discussed.

7.1 Paper I – Poly(styrene)-*block*-Maltoheptaose Films for Sub-10 nm Pattern Transfer: Implications for Transistor Fabrication

7.1.1 Background

The EU project GreeNanoFilms [23] have made efforts towards sustainability for next generation nanolithography. Part of the project was sub-10 nm patterning using a carbohydrate-based BCP for e.g., SERS bio-sensor applications. Even though a high dry etch selectivity of 14:1 between homo-polymer blankets of MH over PS could be found in CF_4/O_2 (3:1) plasma RIE [183], there were difficulties in removing the sacrificial component from PS-*b*-MH. Therefore, another strategy was formed. The hypothesis was that MH could be selectively infiltrated with alumina by sequential infiltration synthesis using TMA and water, analogous with the case with the well-explored PS-*b*-PMMA [155]. After removal of the polymer matrix, the remaining hybrid material features might be able to serve as an etch mask for pattern transfer [16].

7.1.2 Results

Low molecular weight and high-χ PS-*b*-MH (4.5k-*b*-1.2k) was self-assembled in thin films on top of silicon substrates to either vertical or horizontal MH cylinders of a pattern periodicity of 12 nm. By using multiple precursor pulses of TMA and water, containing aluminium and oxygen, respectively, it was possible to selectively create alumina rich features at the positions of MH. It was concluded that the alumina rich feature dimensions increased with the number of infiltration cycles, to be 5-6 nm after eight cycles. Dry etching in a low-pressure plasma from Ar and Cl_2 successfully removed the polymer matrix, without distorting the pattern (see **Figure 23**). However, also part of the hybrid material mask was etched during the process, resulting in a thin

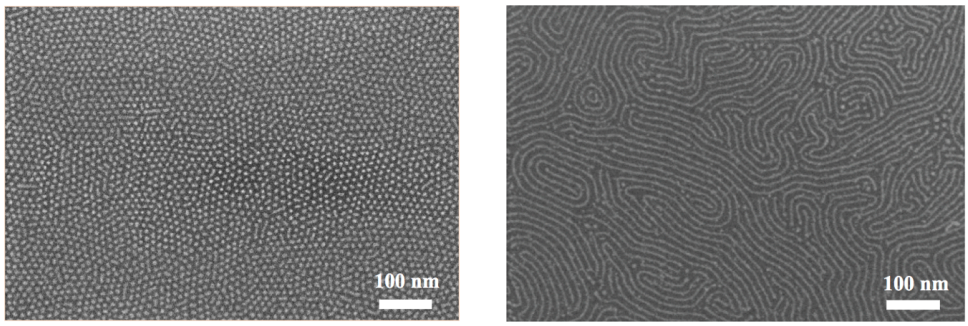

Figure 23. Top view SEM images of alumina infiltrated PS-*b*-MH after polymer removal. To the left, vertical cylinders, and to the right, horizontal cylinders.

remaining mask. Therefore, another polymer removal process was optimized using a gentle low-pressure O_2 plasma. Thereafter, pattern transfer into silicon to an aspect ratio of 2:1 was possible to perform in low-pressure $SF_6/C_4F_8/Ar$ (26:54:20) plasma. The resulting trenches were approximately 5 nm in width and 10 nm in depth (see **Figure 24**).

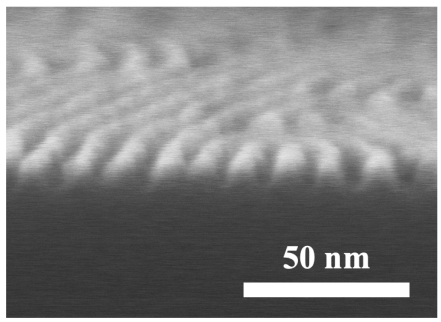

Figure 24. Cross-sectional SEM image of pattern transferred 12 nm pitch PS-*b*-MH into Si.

To investigate the infiltration selectivity, efficiency, and depth, ex-situ specular neutron reflectivity was used of infiltrated homopolymer blanket films of MH and hydroxyl-terminated PS (PS-OH). Eight cycles of multiple pulse infiltration resulted in an alumina content corresponding to 23 vol% of included Al_2O_3 to a depth of 2.5 nm in a MH blanket film, whereas the content in the PS-OH film corresponded to 0.8 vol% Al_2O_3 to the full depth of 19 nm. A brief comparison to a semi-static infiltration process showed a similar performance, although using approximately 60 times less precursor material.

7.1.3 Discussion and implications

The reaction mechanism has not been verified but could potentially be investigated using in-situ FTIR. However, the hypothesis is that the Lewis acid TMA reacts with the hydroxyl groups of MH, acting as Lewis base, in analogy with the reaction with e.g., 4-hydroquinone [108]. Successful SIS into MH using TMA and water implies that also other carbohydrate-based polymers, including hydroxyl functional groups, should be possible to infiltrate with inorganic material. Furthermore, PS without contamination or entrapment of precursors is inert to TMA and water infiltration [154]. The use of PS-OH for the infiltration investigation also enabled exploration of the infiltration depth into PS. It should be noted that PS without hydroxyl-termination should have a better infiltration selectivity to MH.

Enabling lithography and pattern transfer methods into silicon at 12 nm pitch could potentially have an enormous impact on e.g., FinFETs, where the so-called 3 nm node technology is predicted to use 24 nm fin pitch [27]. Furthermore, a successful pattern transfer into silicon, followed by a thin gold deposition, might create a surface, suitable for enhancing plasmonic resonance in a high sensitivity SERS sensor.

7.1.4 Concluding remarks

Specular neutron reflectometry was for the first time used to investigate SIS of inorganic material into polymer thin films. Sequential infiltration synthesis of TMA and water into MH to form an alumina-like hybrid material has not previously been shown. The infiltration process overcomes the difficulty to remove the sacrificial component of PS-*b*-MH, despite the fact that the interface region between the two blocks is expected to be proportionally large, which is a known challenge for BCP lithography and pattern transfer in the sub-10 nm regime [37]. Pattern transfer into silicon at 12 nm pitch using the hybrid material features as an etch mask could potentially have a great impact on future device fabrication.

7.2 Paper II – Sequential Infiltration Synthesis into Maltoheptaose and Poly(styrene): Implications for sub-10 nm Pattern Transfer

7.2.1 Background

Paper I showed potential for sub-10 nm pattern transfer into silicon using SIS with TMA and water precursors into PS-*b*-MH and indicated that semi-static infiltration could be a more precursor material efficient method. An investigation of semi-static SIS process parameters to increase the understanding of the infiltration process into MH and to optimize the alumina content and material selectivity to PS was therefore initiated.

7.2.2 Results

From specular neutron reflectivity measurements, it was indicated that the maximum alumina infiltration content is to be found between 64°C and 100°C. By decreasing the precursor exposure time to 20 s, the alumina content was increased to 40 vol%, but at the expense of decreasing infiltration depth, which was then only 1.4 nm (see **Figure 25**). Increasing the precursor pulse durations to 75/45 ms for TMA/water i.e., increasing precursor partial pressure, resulted in an increase in the alumina content to 40 vol% in MH and only 1.5 nm infiltration depth. A similar result was found when decreasing the pulse duration to 10/5 ms. The infiltration selectivity to PS-OH was maintained for all investigated process parameters.

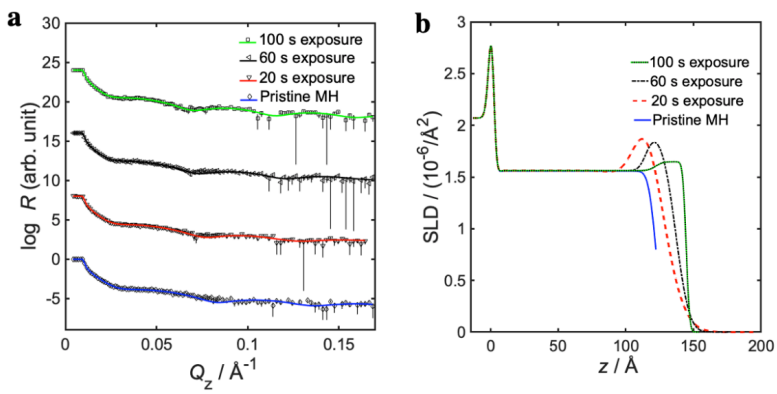

Figure 25. Data from neutron reflectometry of MH at various SIS exposure times. a) showing measured specular neautron reflectivity, error, and fitted model as a function of neutron momentum transfer perpendicular to the sample surface, and b) showing modelled scattering length density as a function of distance to substrate. Reproduced with permission from the Authors of **Paper II**. Copyright 2021 by the Authors.

7.2.3 Discussion and implications

An optimum SIS temperature for TMA and MH should be close to 80°C. The balance point, where forward and reverse reaction rates are equal, have previously been shown to infiltrate TMA into both PMMA and P2VP with maximum mass gain at thermal equilibrium [113]. The balance point for MH might therefore be positioned between 64°C and 100°C. It should, however, be noted that the errors are in the same order as the differences. Furthermore, the optimum precursor exposure time might be between 20 s and 60 s, with a trade-off for a high alumina content and a deeper infiltration. A short pulse duration of 10/5 ms TMA/water will minimize the amount of used precursor material, and at the same time give a high infiltration selectivity.

7.2.4 Concluding remarks

No study of the effect of the process parameters temperature, exposure time, and pulse duration on infiltration using TMA and water into MH have previously been made. These results will enable further understanding of the process, and optimization of the process of SIS of TMA and water into PS-*b*-MH for sub-10 nm pattern transfer. By changing the process from the dynamic process used in **Paper I** to the semi-static process parameters without further optimization, the precursor amount was decreased approximately 600 times, whereas the alumina content of the MH blanket film increased by 9%. By increasing the amount of alumina in the infiltrated MH cylinders possibilities of enabling a higher aspect ratio pattern transfer into silicon is dramatically increased.

7.3 Paper III – Feature size control using surface reconstruction temperature in block copolymer lithography for InAs nanowire growth

7.3.1 Background

Development of high technology devices was predicted by Moore to increase in components per circuit, at the same time as the cost per component would be lowered [26]. As this prediction was first made in the 1960s, interpretation of what is commonly known as Moore's law has changed over time, but a more modern view predicts an increasing performance at reduced power, and still maintains that the number of devices per footprint area should increase, at the same time as cost per device should decrease [27]. One route to increase the number of devices per footprint area is introducing vertical III-V transistors, predicted as a possible future industrial technology by the international roadmap for devices and systems (IRDS) [27]. The IRDS also states that is important to maintain control over the parasitic effects. By reducing the vertical nanowire (VNW) spacing, we can, apart from increasing device density, also reduce the parasitic capacitances in nanowire transistors, allowing for high frequency operation [184]. To accommodate for the dense packing, the nanowire diameter may also decrease. By doing so, the transistor electrostatics, such as sub-threshold slope, will also improve [185]. However, it has been found that at room temperature, the field effect electron mobility reduces linearly with the InAs diameter [186]. Furthermore, using selective area epitaxy, instead of VLS, would eliminate gold from the processing, which would be beneficial for sustainability reasons, as well as for minimizing the risk of semiconductor gold deep-level doping [187], thus making the processing potentially industrially CMOS compatible [168, 178]. Furthermore, selective area epitaxy enables abrupt junction transitions [141]. The experimental strategy was to optimize processes for selective area template openings patterned using a high-χ BCP, with possibilities to downscale dimensions.

7.3.2 Results

An investigation of surface reconstruction in ethanol of self-assembled PS-*b*-P4VP (50k-*b*-17k) thin films on top of silicon nitride showed the possibility to control the mean pore diameter by varying ethanol temperature. Already after 15 minutes of surface reconstruction in ethanol, the mean pore diameter reached 12 nm at 18°C and 23 nm at 60°C, not changing much after that time. At 15 minutes, the mean pitch was 49-50 nm for all investigated temperatures. After 4 h surface reconstruction, the mean pitch showed a tendency to increase with temperature, from 43 nm at 18°C to 50 nm

at 60°C. At 70°C the morphology was completely altered, to an almost flat surface. Furthermore, it was showed that a size dependence on surface reconstruction temperature was maintained also after removal of polymer layer in O_2 plasma RIE to enable pattern transfer.

Pattern transfer was performed into silicon nitride using CHF_3/N_2 (1:4) plasma RIE, and wet etching, to create a selective area template. The MOVPE of InAs nanowires was made from the template, on a silicon platform with an InAs buffer layer atop, grown using arsine/TMIn at a V/III ratio of 5 at 550°C. When using 60°C surface reconstruction temperature, the mean diameter of the silicon nitride template openings was 25 nm, whereas the VNWs were 32 nm at the top, across the slowest growing facets, and the pitch was 50 nm. The nanowire yield was varying within substrates; however, the concept was demonstrated.

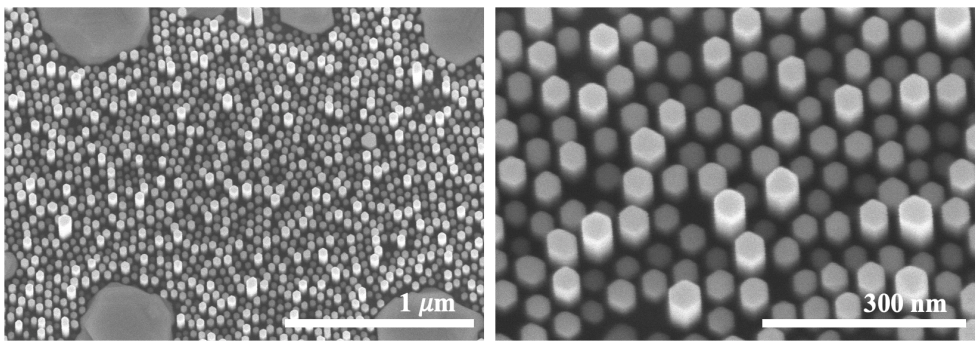

Figure 26. SEM images in 5° tilted view of selective area MOVPE InAs nanowires. Grown using BCP templated pattern transferred openings in a silicon nitride mask.

7.3.3 Discussion and implications

It was shown that the resulting lithographic feature size can be finetuned for a fix molecular weight PS-*b*-P4VP by altering the surface reconstruction temperature, providing an unusual flexibility. The fact that the pitch was changing with time and temperature during surface reconstruction of PS-*b*-P4VP in ethanol is an indication of some degree of solubility of PS in ethanol. Furthermore, the largest process window was found for 40°C surface reconstruction temperature, since it left the mean pitch stable at 49 nm for all investigated durations. Also, the mean pore size was 17-19 nm at that temperature.

7.3.4 Concluding remarks

Although the use of ethanol for surface reconstruction has been previously reported [188], this is the first systematic study of the dependence of pore size on temperature. The used PS-*b*-P4VP had a polydispersity of 1.15, which is rather high.

By using a BCP with a polydispersity closer to 1, a better pattern size uniformity should be possible to achieve. Further optimization of the SVA process, and contamination assessment, could also be useful for uniformity improvement. A varying diameter of the openings in the selective area epitaxy template will lead to varying VNW diameter and length. For the first time, VNW epitaxy is reported with a process using the high-χ material PS-*b*-P4VP. This material is reported to self-assemble lamellae at 10.3 nm pitch [189], why downscaling BCP feature size is feasible. The use of silicon nitride as template reduces the risk of oxygen contamination of the nanowire channels. The process is also developed on a silicon platform, excluding gold, aiming for CMOS compatibility.

7.4 Paper IV – Directed Self-Assembly for Dense Vertical III-V Nanowires on Si and Implications for Gate All-Around Deposition

7.4.1 Background

Paper III showed the possibilities of using PS-*b*-P4VP to make selective area templates for growth of III-V vertical nanowires. The target was to further develop the processing towards vertical transistor device fabrication. An increased nanowire yield, control of nanowire positioning, and possibilities for subsequent processing were identified as key points. Vertical nanowire gate all-around (GAA) FETs have previously been shown to potentially have lower parasitic resistance and capacitance and reduced power consumption compared to lateral nanowire GAA-FETs, or triple-gate FinFETs [190], why investigation of gate all-around deposition possibilities of BCP defined selective area MOVPE templates was of interest. Furthermore, as the negative EBL resist hydrogen silesquioxane (HSQ) was previously shown to be suitable as template for MOVPE growth [191], it motivated the use of it as guiding pattern material.

7.4.2 Results

By use of guiding patterns in HSQ of 50 nm line width, the self-assembly of 50 nm pitch PS-*b*-P4VP could be directed in respect to the <112> crystal direction of the substrate. This enabled two types of VNW configurations after growth – one with more triangular spacing, the so-called star configuration, and one with more equidistant spacing, the so-called sun configuration. The self-assembly was made at short range in number of rows spanning from 0 to approximately 8 by varying the guiding pattern gap size. Both the nanowire row pitch and the nanowire width were affected by gap size. Furthermore, the nanowire yield was increased from **Paper III** (see **Figure 27a**). A distribution of nanowire diameter and nanowire length remained, although the distribution decreased somewhat in areas with better uniformity from DSA. Nanowires growing close to guiding pattern edges were somewhat longer, likely due to excess precursor material.

To further evaluate processing possibilities at these extreme conditions, atomic layer deposition of typical high-κ gate oxide AlO_x/HfO_x and gate metal TiN_x was made, to make deposition as conformal as possible. After gate all-around deposition, the nanowire spacing was extremely small (see **Figure 27b**), and the nanowire TiN_x layers were frequently touching in both star and sun configuration (see **Figure 27c** and **d**).

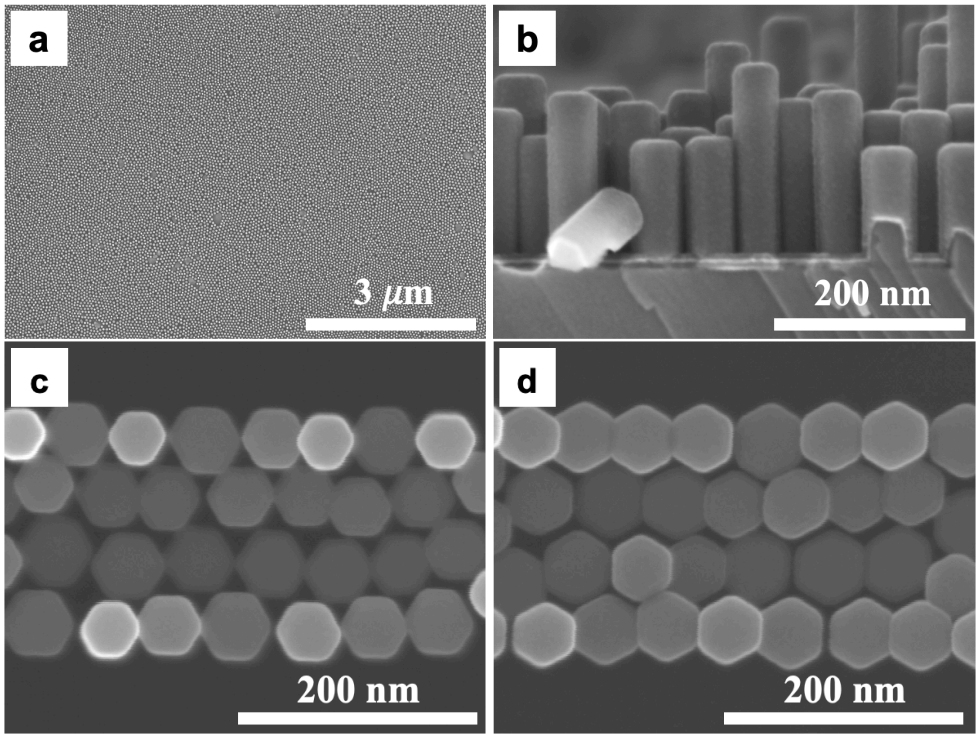

Figure 27. SEM images of vertical nanowires. a) Top view image of InAs nanowires after growth in free self-assembly area, **b)** cross-sectional image of InAs nanowires in free self-assembly areas after deposition of high-κ and TiN_x, **c)** top view image in DSA area of 4 rows of InAs nanowires in so-called star configuration after deposition of high-κ and TiN_x, and **d)** top view image in DSA area of 4 rows of InAs nanowires in so-called sun configuration after deposition of high-κ and TiN_x. Adapted with permission from the Authors of **Paper IV**. Copyright 2021 by the Authors.

7.4.3 Discussion and implications

The self-assembly was made in number of rows spanning from 0 to approximately 8, with an overlap between number of rows, by selecting a gap size corresponding to the number of rows that fit according to the commensurability condition, in line with the work of Cheng et al. [80]. By making several changes in the overall process, the nanowire yield was increased from the results in **Paper III**. Deposition of template material, solvent proportions in BCP mixture, SVA solvent proportions, surface reconstruction temperature, using wet etching of last part of template, and change of wet etchant prior to growth might all have contributed to the improved yield. Furthermore, InAs has great potential for device fabrication, as it has a high electron mobility [186], and the high-κ and TiN_x layers were deposited according to current transistor processing considerations [145, 192, 193].

7.4.4 Concluding remarks

The tight spacing between nanowires makes subsequent processing less straight forward. By demonstrating gate all-around deposition for the two nanowire configurations, crucial steps in highly dense vertical nanowire transistor fabrication have been clarified. These results are expected to be of use for further transistor development. Future investigations could include complete transistor fabrication and electrical characterization.

8 Concluding Remarks

BCP lithography has some limitations and challenges, but also huge potential as a future patterning technique for high technology devices. This chapter will briefly review some of them.

8.1 Current Limitations/Challenges

A hot topic in the BCP community is reduction of defects in DSA and pattern transfer. The line edge roughness (LER) and the self-assembly defects, such as bridging, disclinations, and dislocations, often needs to be minimized to pass the requirements of the industry [25, 70, 194]. Furthermore, the polymer should be synthesized in such a way, that the polydispersity [28] is low, to minimize the pattern dimension variation, and the synthesis should preferably be metal free, as any remaining metal contamination could be critical to e.g., an electronic device, due to deep-level doping [195].

Even if BCPs can be self-assembled into sub-10 nm patterns, it does not automatically mean they can be pattern transferred. Due to the relatively long block-to-block interface region of sub-10 nm BCP features [37] developing methods to achieve pattern transfer at this resolution is a challenge.

One drawback of BCP lithography, is the morphology limitations. Mixing and matching of various pattern types on the same substrate requires more thought and processing steps than direct writing lithography techniques, such as EBL. Also, the BCP self-assembly is often rather substrate surface energy sensitive, why it is beneficial to be aware of the existing processing window, and of the effect of process change.

8.2 Advantages

The ability of BCPs to self-assemble into patterns in the sub-10 nm range motivates research on how to optimize the technology further. For example, IRDS has identified BCP lithography using DSA as a potential technique for reaching sub-7 nm patterning of devices [178], and the potential use of high density patterns is vast.

Another advantage of BCP lithography is the possibility to rectify patterns [78], to improve subsequent pattern transfer made with other lithography techniques. This is closely related to downscaling of via holes [83]. The BCP lithography would then be a technique added to another lithography method, to improve pattern quality and/or decrease feature sizes.

BCP self-assembly does not require expensive equipment and can thus be performed in a low budget lab. The process complexity does essentially not scale with wafer size but remains approximately the same. This supports BCP lithography being a low-cost technique. Furthermore, a self-assembled BCP monolayer will have a rather even polymer thickness, facilitating an even pattern transfer over large areas.

9 Outlook

Continued research within the field of BCP lithography and nanofabrication could be very rewarding, and there are numerous paths to do so. This chapter includes a few suggestions for future research.

9.1 Self-Assembly and Sub-10 nm Pattern Transfer

A study on surface energy variations [60] e.g., using self-assembled monolayers and BCP self-assembly could lead to further improved chemo-epitaxial DSA strategies, as well as increased processing windows. Exploration of triblock copolymer self-assembly morphologies [45] and possibilities for sacrificial component processes could improve high-resolution capabilities [30].

Increase of long-range order, and enabling of localized patterned areas, using DSA, potentially by Talbot displacement lithography [196], nanoimprint lithography (NIL) [82], UV lithography [197], and/or EBL. One example could be patterned hole shrink [83], using Talbot displacement combined with BCP lithography. Another goal could be to clearly define a local MOVPE growth area of the vertical nanowires, to facilitate transistor processing.

Integration of in-situ film thickness measurement tool in the custom built SVA chamber [56], controlling chamber pressure, introducing the solvent vapor using bubblers, and monitoring the BCP film thickness [152], similar to the work by Gotrik et al. [50], could be a strategy for reducing SVA duration, and for improving self-assembly control. Exploring the possibility of elevated substrate temperatures to enable solvothermal annealing should reduce annealing times further [55].

Investigation on high-χ BCP systems suitable for infiltration and/or pattern transfer should be continued e.g., PS-*b*-MH, PS-*b*-P4VP, or PDMS-*b*-PLA. Furthermore, cryo-etching of sub-10 nm patterns could drastically change the possible aspect ratios in pattern transfer [129]. Investigation of selective P4VP dry etch removal for pattern transfer [13] could be one option. Exploration of selective laser ablation of MH [14] might show useful. One advantage of using PDMS is that it will turn into a carbon containing silicon dioxide like material, when it undergoes oxygen plasma RIE [198], at the same time as e.g., PLA will be removed. If PDMS is the majority block,

there would be great possibilities for both pattern transfer and SA-MOVPE. Researching sub-10 nm pattern transfer could potentially have a great impact for society.

9.2 Sequential Infiltration Synthesis

Exploration of new combinations of precursors and polymers in SIS, where the hybrid material could be part of the device would be interesting e.g., creating a high-κ hybrid material using a hafnium-containing precursor and water/oxygen. Furthermore, in-situ QCM and/or FTIR investigation [155] of the TMA and water infiltration into MH, in combination with density functional theory calculations [199] could shed light on the reaction mechanisms. Also, use of ex-situ FTIR and EDS techniques might be rewarding.

9.3 Vertical and Lateral Transistors

Next, implementation of the developed VNW process to existing transistor processes could be tested, and electrical characterization performed. Presently, the grown InAs nanowires are varying in length, and polishing or etching could be explored to level them. It would also be interesting to investigate the possibilities of growing III-V fins from a BCP defined mask in MOVPE. Furthermore, pattern transfer of BCP defined patterns into a wider variety of materials, such as III-V for FinFET fabrication.

9.4 Nanoimprint Lithography

Pattern transfer of a BCP lithography pattern into silicon could be used as a mold for nanoimprint lithography (NIL), after polymer strip and anti-sticking treatment. Furthermore, NIL for DSA [82] could be performed in several ways e.g., by imprinting the BCP directly [200], which could be interesting also from a cost-reducing high-volume perspective.

9.5 Characterization

Future work could be to further develop neutron reflectometry of the selectively alumina infiltrated PS-*b*-MH, along with homopolymer films, expanding to larger

angles to further decrease the number of possible fits to a data set, but also by performing in-situ experiments. Consideration of using deuterated BCP for increased contrast could be made. Further investigations in how grazing incidence small-angle neutron scattering (GISANS) might be beneficial for infiltration characterization is also suggested. Use of grazing incidence small-angle X-ray scattering (GISAXS) should also provide lateral insight on self-assembly, infiltration and nanowire growth. An in-situ inspection would be most informative.

Inspection of BCPs in cross-section is rarely done [70]. This can be performed in SEM. There is, however, a risk of damages during sample preparation, as well as during inspection. Sample preparation for TEM of infiltrated BCPs can be explored. Inspection of structures at sub-10 nm dimensions is often challenging, especially when lateral resolution regarding chemical composition is desired. All development in a direction facilitating this could be appreciated also by researcher in related fields.

References

[1] T. Jagannathan, *Micro/Nanolithography - A Heuristic Aspect on the Enduring Technology*. IntechOpen, **2018**.

[2] N. Mojarad, M. Hojeij, L. Wang, J. Gobrecht, and Y. Ekinci, "Single-digit-resolution nanopatterning with extreme ultraviolet light for the 2.5 nm technology node and beyond," *Nanoscale,* vol. 7, no. 9, pp. 4031-4037, **2015**.

[3] P. D. Bisschop and E. Hendrickx, "Stochastic effects in EUV lithography," in *Proc.SPIE*, 2018, vol. 10583: SPIE, in SPIE proceedings, **2018**, p. 105831K.

[4] V. R. Manfrinato, L. Zhang, D. Su, H. Duan, R. G. Hobbs, E. A. Stach, and K. K. Berggren, "Resolution Limits of Electron-Beam Lithography toward the Atomic Scale," vol. 13, ed, **2013**, pp. 1555-1558.

[5] W. F. van Dorp, B. van Someren, C. W. Hagen, P. Kruit, and P. A. Crozier, "Approaching the Resolution Limit of Nanometer-Scale Electron Beam-Induced Deposition," *Nano Letters,* vol. 5, no. 7, pp. 1303-1307, **2005**.

[6] T. H. P. Chang, "Proximity effect in electron-beam lithography," Place of Publication: Colorado Springs, CO, USA. Country of Publication: USA., 1976/11/01/ 1975, vol. 12: American Vacuum Soc. American Vacuum Soc., 6 ed., pp. 1271-1275.

[7] B. J. Ree, Y. Satoh, T. Isono, and T. Satoh, "Correlations of nanoscale film morphologies and topological confinement of three-armed cage block copolymers," *Polymer Chemistry,* vol. 12, no. 23, pp. 3451-3460, **2021**.

[8] C. Harrison, J. A. Dagata, and D. H. Adamson, "Lithography with Self-Assembled Block Copolymer Microdomains," in *Developments in Block Copolymer Science and Technology*, **2004**, pp. 295-323.

[9] P. Mansky, P. haikin, and E. L. Thomas, "Monolayer films of diblock copolymer microdomains for nanolithographic applications," *Journal of Materials Science,* vol. 30, no. 8, pp. 1987-1992, **1995**.

[10] P. Mansky, C. K. Harrison, P. M. Chaikin, R. A. Register, and N. Yao, "Nanolithographic templates from diblock copolymer thin films," *Applied Physics Letters,* vol. 68, no. 18, pp. 2586-2588, **1996**.

[11] M. Park, C. Harrison, P. M. Chaikin, R. A. Register, and D. H. Adamson, "Block copolymer lithography: Periodic arrays of ~1011 holes in 1 square centimeter," *Science,* vol. 276, no. 5317, pp. 1401-1404, **1997**.

[12] F. S. Bates and G. H. Fredrickson, "Block Copolymer Thermodynamics: Theory and Experiment," *Annual Review of Physical Chemistry,* vol. 41, no. 1, p. 525, **1990**.

[13] S. P. Flynn, J. Bogan, R. Lundy, K. E. Khalafalla, M. Shaw, B. J. Rodriguez, P. Swift, S. Daniels, R. O'Connor, G. Hughes, and S. M. Kelleher, "Nitrogen reactive ion etch processes for the selective removal of poly-(4-vinylpyridine) in block copolymer films," *Nanotechnology,* vol. 29, no. 35, p. 355302, **2018**.

[14] D. L. Olynick, P. Perera, A. Schwartzberg, P. Kulshreshta, D. G. De Oteyza, N. Jarnagin, C. Henderson, Z. Sun, I. Gunkel, T. Russell, M. Budden, and I. W. Rangelow, "Selective laser ablation in resists and block copolymers for high resolution lithographic patterning," *Journal of Photopolymer Science and Technology,* vol. 28, no. 5, pp. pp. 663-668, **2015**.

[15] E. Cara, I. Murataj, G. Milano, N. De Leo, L. Boarino, and F. Ferrarese Lupi, "Recent Advances in Sequential Infiltration Synthesis (SIS) of Block Copolymers (BCPs)," *Nanomaterials,* vol. 11, no. 4, **2021**.

[16] C. Cummins, T. Ghoshal, J. D. Holmes, and M. A. Morris, "Strategies for Inorganic Incorporation using Neat Block Copolymer Thin Films for Etch Mask Function and Nanotechnological Application," *Advanced Materials,* vol. 28, no. 27, pp. 5586-5618, **2016**.

[17] A. Nunns, J. Gwyther, and I. Manners, "Inorganic block copolymer lithography," *Polymer,* vol. 54, no. 4, pp. 1269-1284, **2013**.

[18] T. Xu, J. Stevens, J. A. Villa, J. T. Goldbach, K. W. Guarini, C. T. Black, C. J. Hawker, and T. P. Russell, "Block Copolymer Surface Reconstuction: A Reversible Route to Nanoporous Films," *Advanced Functional Materials,* vol. 13, no. 9, pp. 698-702, **2003**.

[19] Y. Wang and F. Li, "An Emerging Pore-Making Strategy: Confined Swelling-Induced Pore Generation in Block Copolymer Materials," *Advanced Materials,* vol. 23, no. 19, pp. 2134-2148, **2011**.

[20] S.-K. Kim, D.-G. Kim, A. Lee, H.-S. Sohn, J. J. Wie, N. A. Nguyen, M. E. Mackay, and J.-C. Lee, "Organic/Inorganic Hybrid Block Copolymer Electrolytes with Nanoscale Ion-Conducting Channels for Lithium Ion Batteries," *Macromolecules,* vol. 45, no. 23, pp. 9347-9356, **2012**.

[21] W.-S. Young, W.-F. Kuan, and I. I. I. T. H. Epps, "Block copolymer electrolytes for rechargeable lithium batteries," *Journal of Polymer Science Part B: Polymer Physics,* vol. 52, no. 1, pp. 1-16, **2014**.

[22] C.-C. Kuo, Y.-C. Tung, and W.-C. Chen, "Morphology and pH Sensing Characteristics of New Luminescent Electrospun Fibers Prepared from Poly(phenylquinoline)-block-Polystyrene/Polystyrene Blends," *Macromolecular Rapid Communications,* vol. 31, no. 1, pp. 65-70, **2010**.

[23] "GreeNanoFilms European Project." http://www.greenanofilms.eu/ (accessed September 9, 2021).

[24] I. Otsuka, S. Tallegas, Y. Sakai, C. Rochas, S. Halila, S. Fort, A. Bsiesy, T. Baron, and R. Borsali, "Control of 10 nm scale cylinder orientation in self-organized sugar-based block copolymer thin films," *Nanoscale,* vol. 5, no. 7, pp. 2637-2641, **2013**.

[25] C.-C. Liu, E. Franke, Y. Mignot, R. Xie, C. W. Yeung, J. Zhang, C. Chi, C. Zhang, R. Farrell, K. Lai, H. Tsai, N. Felix, and D. Corliss, "Directed self-assembly of block copolymers for 7 nanometre FinFET technology and beyond," *Nature Electronics,* vol. 1, no. 10, pp. 562-569, **2018**.

[26] G. E. Moore, "Cramming more components onto integrated circuits, Reprinted from Electronics, volume 38, number 8, April 19, 1965, pp.114 ff," *IEEE Solid-State Circuits Society Newsletter,* vol. 11, no. 3, pp. 33-35, **2006**.

[27] "International Roadmap for Devices and Systems, 2020 Update, More Moore." IEEE. https://irds.ieee.org/editions/2020/more-moore (accessed 1 April 2021).

[28] J. M. G. Cowie and V. Arrighi, *Polymers : chemistry and physics of modern materials*, 3. ed. ed. CRC Press, **2008**.

[29] Y. Matsushita, "Block Copolymers," in *Encyclopedia of Polymeric Nanomaterials*, S. Kobayashi and K. Müllen Eds. Berlin, Heidelberg: Springer Berlin Heidelberg, **2014**, pp. 1-5.

[30] S. Xiong, L. Wan, Y. Ishida, Y.-A. Chapuis, G. S. W. Craig, R. Ruiz, and P. F. Nealey, "Directed Self-Assembly of Triblock Copolymer on Chemical Patterns for Sub-10-nm Nanofabrication via Solvent Annealing," *ACS Nano,* vol. 10, no. 8, pp. 7855-7865, **2016**.

[31] W. Zheng and Z.-G. Wang, "Morphology of ABC Triblock Copolymers," *Macromolecules,* vol. 28, no. 21, pp. 7215-7223, **1995**.

[32] Z. Guo, G. Zhang, F. Qiu, H. Zhang, Y. Yang, and A.-C. Shi, "Discovering Ordered Phases of Block Copolymers: New Results from a Generic Fourier-Space Approach," *Physical Review Letters,* vol. 101, no. 2, p. 028301, **2008**.

[33] Z. Sun, W. Zhang, S. Hong, Z. Chen, X. Liu, S. Xiao, E. B. Coughlin, and T. P. Russell, "Using block copolymer architecture to achieve sub-10 nm periods," *Polymer,* vol. 121, pp. 297-303, **2017**.

[34] K. Sugiyama, "Block Copolymer Synthesis," in *Encyclopedia of Polymeric Nanomaterials*, S. Kobayashi and K. Müllen Eds. Berlin, Heidelberg: Springer Berlin Heidelberg, **2014**, pp. 1-10.

[35] A. Löfstrand, R. Jafari Jam, K. Mothander, T. Nylander, M. Mumtaz, A. Vorobiev, W.-C. Chen, R. Borsali, and I. Maximov, "Poly(styrene)-block-Maltoheptaose Films for Sub-10 nm Pattern Transfer: Implications for Transistor Fabrication," *ACS Applied Nano Materials,* vol. 4, no. 5, pp. 5141-5151, **2021**.

[36] S. B. Darling, "Directing the self-assembly of block copolymers," *Progress in Polymer Science,* vol. 32, no. 10, pp. 1152-1204, **2007**.

[37] L. Wan, R. Ruiz, H. Gao, K. C. Patel, T. R. Albrecht, J. Yin, J. Kim, Y. Cao, and G. Lin, "The Limits of Lamellae-Forming PS-b-PMMA Block Copolymers for Lithography," *ACS Nano,* vol. 9, no. 7, pp. 7506-7514, **2015**.

[38] C. Sinturel, F. S. Bates, and M. A. Hillmyer, "High χ–Low N Block Polymers: How Far Can We Go?," *ACS Macro Letters,* vol. 4, no. 9, pp. 1044-1050, **2015**.

[39] M. D. Rodwogin, C. S. Spanjers, C. Leighton, and M. A. Hillmyer, "Polylactide−Poly(dimethylsiloxane)−Polylactide Triblock Copolymers as Multifunctional Materials for Nanolithographic Applications," *ACS Nano,* vol. 4, no. 2, pp. 725-732, **2010**.

[40] E. W. Cochran, C. J. Garcia-Cervera, and G. H. Fredrickson, "Stability of the Gyroid Phase in Diblock Copolymers at Strong Segregation," *Macromolecules,* vol. 39, no. 7, pp. 2449-2451, **2006**.

[41] E. Kim, H. Ahn, S. Park, H. Lee, M. Lee, S. Lee, T. Kim, E.-A. Kwak, J. H. Lee, X. Lei, J. Huh, J. Bang, B. Lee, and D. Y. Ryu, "Directed Assembly of High Molecular Weight Block Copolymers: Highly Ordered Line Patterns of Perpendicularly Oriented Lamellae with Large Periods," *ACS Nano,* vol. 7, no. 3, pp. 1952-1960, **2013**.

[42] H. Jung, T. Jun, W. Lee, and D. Y. Ryu, "Ordering and Orientation of Giant Nanostructures from High-Molecular-Weight Block Copolymer via Solvent Vapor Annealing Process," *Journal of Photopolymer Science and Technology,* vol. 31, no. 4, pp. 479-482, **2018**.

[43] I. Botiz and S. B. Darling, "Optoelectronics using block copolymers," *Materials Today,* vol. 13, no. 5, pp. 42-51, **2010**.

[44] C. Tang, E. M. Lennon, G. H. Fredrickson, E. J. Kramer, and C. J. Hawker, "Evolution of Block Copolymer Lithography to Highly Ordered Square Arrays," *Science,* vol. 322, p. 429, **2008**.

[45] S. Li, Y. Jiang, and J. Z. Y. Chen, "Morphologies and phase diagrams of ABC star triblock copolymers confined in a spherical cavity," *Soft Matter,* vol. 9, no. 19, pp. 4843-4854, **2013**.

[46] F. S. Bates and G. H. Fredrickson, "Block Copolymer Thermodynamics: Theory and Experiment," *Annual Review of Physical Chemistry,* vol. 41, no. 1, pp. 525-557, **1990**.

[47] I. Otsuka, T. Isono, C. Rochas, S. Halila, S. Fort, T. Satoh, T. Kakuchi, and R. Borsali, "10 nm Scale Cylinder–Cubic Phase Transition Induced by Caramelization in Sugar-Based Block Copolymers," *ACS Macro Letters,* vol. 1, no. 12, pp. 1379-1382, **2012**.

[48] K. W. Guarini, C. T. Black, and S. H. I. Yeung, "Optimization of Diblock Copolymer Thin Film Self Assembly," *Advanced Materials,* vol. 14, no. 18, pp. 1290-1294, **2002**.

[49] Hansen, *Hansen Solubility Parameters, A User's Hand- book*. CRC Press, **2000**.

[50] K. W. Gotrik, A. F. Hannon, J. G. Son, B. Keller, A. Alexander-Katz, and C. A. Ross, "Morphology Control in Block Copolymer Films Using Mixed Solvent Vapors," *ACS Nano,* vol. 6, no. 9, pp. 8052-8059, **2012**.

[51] H. Hulkkonen, T. Salminen, and T. Niemi, "Automated solvent vapor annealing with nanometer scale control of film swelling for block copolymer thin films," *Soft Matter,* vol. 15, no. 39, pp. 7909-7917, **2019**.

[52] S. O'Driscoll, G. Demirel, R. A. Farrell, T. G. Fitzgerald, C. O'Mahony, J. D. Holmes, and M. A. Morris, "The morphology and structure of PS-b-P4VP block copolymer films by solvent annealing: Effect of the solvent parameter," *Polymers for Advanced Technologies,* vol. 22, no. 6, pp. 915-923, **2011**.

[53] X. Zhang, K. D. Harris, N. L. Y. Wu, J. N. Murphy, and J. M. Buriak, "Fast Assembly of Ordered Block Copolymer Nanostructures through Microwave Annealing," *ACS Nano,* vol. 4, no. 11, pp. 7021-7029, **2010**.

[54] Y. Liao, W. C. Chen, and R. Borsali, "Carbohydrate-Based Block Copolymer Thin Films: Ultrafast Nano-Organization with 7 nm Resolution Using Microwave Energy," *Advanced Materials,* vol. 29, no. 35, p. 6, **2017**.

[55] K. W. Gotrik and C. A. Ross, "Solvothermal Annealing of Block Copolymer Thin Films," *Nano Letters,* vol. 13, no. 11, pp. 5117-5122, **2013**.

[56] G. Nelson, C. S. Drapes, M. A. Grant, R. Gnabasik, J. Wong, and A. Baruth, "High-Precision Solvent Vapor Annealing for Block Copolymer Thin Films," *Micromachines,* vol. 9, no. 6, p. 271, **2018**.

[57] M. A. Chavis, D.-M. Smilgies, U. B. Wiesner, and C. K. Ober, "Widely Tunable Morphologies in Block Copolymer Thin Films Through Solvent Vapor Annealing Using Mixtures of Selective Solvents," *Advanced functional materials,* vol. 25, no. 20, pp. 3057-3065, **2015**.

[58] R. Lundy, S. P. Flynn, C. Cummins, S. M. Kelleher, M. N. Collins, E. Dalton, S. Daniels, M. A. Morris, and R. Enright, "Controlled solvent vapor annealing

of a high [small chi] block copolymer thin film," *Physical Chemistry Chemical Physics,* vol. 19, no. 4, pp. 2805-2815, **2017**.

[59] J. N. L. Albert, W.-S. Young, R. L. Lewis, T. D. Bogart, J. R. Smith, and T. H. Epps, "Systematic Study on the Effect of Solvent Removal Rate on the Morphology of Solvent Vapor Annealed ABA Triblock Copolymer Thin Films," *ACS Nano,* vol. 6, no. 1, pp. 459-466, **2012**.

[60] J. N. L. Albert and T. H. Epps, "Self-assembly of block copolymer thin films," *Materials Today,* vol. 13, no. 6, pp. 24-33, **2010**.

[61] J. G. Son, K. W. Gotrik, and C. A. Ross, "High-Aspect-Ratio Perpendicular Orientation of PS-b-PDMS Thin Films under Solvent Annealing," *ACS Macro Letters,* vol. 1, no. 11, pp. 1279-1284, **2012**.

[62] J. Hao, Z. Wang, Z. Wang, Y. Yin, R. Jiang, B. Li, and Q. Wang, "Self-Assembly in Block Copolymer Thin Films upon Solvent Evaporation: A Simulation Study," *Macromolecules,* vol. 50, no. 11, pp. 4384-4396, **2017**.

[63] X.-s. Jin, Y.-y. Pang, and S.-x. Ji, "From self-assembled monolayers to chemically patterned brushes: Controlling the orientation of block copolymer domains in films by substrate modification," *Chinese Journal of Polymer Science,* vol. 34, no. 6, pp. 659-678, **2016**.

[64] E. Han, K. O. Stuen, Y.-H. La, P. F. Nealey, and P. Gopalan, "Effect of Composition of Substrate-Modifying Random Copolymers on the Orientation of Symmetric and Asymmetric Diblock Copolymer Domains," *Macromolecules,* vol. 41, no. 23, pp. 9090-9097, **2008**.

[65] L. Oria, A. Ruiz de Luzuriaga, J. A. Alduncin, and F. Perez-Murano, "Polystyrene as a brush layer for directed self-assembly of block co-polymers," *Microelectronic Engineering,* vol. 110, pp. 234-240, **2013**.

[66] R. D. Peters, X. M. Yang, T. K. Kim, and P. F. Nealey, "Wetting Behavior of Block Copolymers on Self-Assembled Films of Alkylchlorosiloxanes: Effect of Grafting Density," *Langmuir,* vol. 16, no. 24, pp. 9620-9626, **2000**.

[67] E. W. Edwards, M. P. Stoykovich, H. H. Solak, and P. F. Nealey, "Long-Range Order and Orientation of Cylinder-Forming Block Copolymers on Chemically Nanopatterned Striped Surfaces," *Macromolecules,* vol. 39, no. 10, pp. 3598-3607, **2006**.

[68] A. Knoll, A. Horvat, K. S. Lyakhova, G. Krausch, G. J. A. Sevink, A. V. Zvelindovsky, and R. Magerle, "Phase Behavior in Thin Films of Cylinder-Forming Block Copolymers," *Physical Review Letters,* vol. 89, no. 3, p. 035501, **2002**.

[69] J. Y. Cheng, C. A. Ross, H. I. Smith, and E. L. Thomas, "Templated Self-Assembly of Block Copolymers: Top-Down Helps Bottom-Up," *Advanced Materials,* vol. 18, no. 19, pp. 2505-2521, **2006**.

[70] M. A. Morris, "Directed self-assembly of block copolymers for nanocircuitry fabrication," *Microelectronic Engineering,* vol. 132, pp. 207-217, **2015**.

[71] W. Li and M. Müller, "Directed self-assembly of block copolymers by chemical or topographical guiding patterns: Optimizing molecular architecture, thin-film properties, and kinetics," *Progress in Polymer Science,* vol. 54-55, pp. 47-75, **2016**.

[72] Y. Chen and S. Xiong, "Directed self-assembly of block copolymers for sub-10 nm fabrication," *International Journal of Extreme Manufacturing,* vol. 2, no. 3, p. 032006, **2020**.

[73] C. Pinto-Gómez, F. Pérez-Murano, J. Bausells, L. G. Villanueva, and M. Fernández-Regúlez, "Directed Self-Assembly of Block Copolymers for the Fabrication of Functional Devices," *Polymers,* vol. 12, no. 10, p. 2432, **2020**.

[74] H. Hu, M. Gopinadhan, and C. O. Osuji, "Directed self-assembly of block copolymers: a tutorial review of strategies for enabling nanotechnology with soft matter," *Soft Matter,* vol. 10, no. 22, pp. 3867-3889, **2014**.

[75] X. Shuaigang, Y. XiaoMin, E. W. Edwards, L. Young-Hye, and P. F. Nealey, "Graphoepitaxy of cylinder-forming block copolymers for use as templates to pattern magnetic metal dot arrays," *Nanotechnology,* vol. 16, no. 7, pp. S324-S329, **2005**.

[76] B. Ion, K. W. Y. Joel, J. Yeon Sik, A. R. Caroline, L. T. Edwin, and K. B. Karl, "Graphoepitaxy of Self-Assembled Block Copolymers on Two-Dimensional Periodic Patterned Templates," *Science,* vol. 321, no. 5891, p. 939, **2008**.

[77] C.-C. Liu, E. Han, M. S. Onses, C. J. Thode, S. Ji, P. Gopalan, and P. F. Nealey, "Fabrication of Lithographically Defined Chemically Patterned Polymer Brushes and Mats," *Macromolecules,* vol. 44, no. 7, pp. 1876-1885, **2011**.

[78] R. Ruiz, H. Kang, F. A. Detcheverry, E. Dobisz, D. S. Kercher, T. R. Albrecht, J. J. de Pablo, and P. F. Nealey, "Density Multiplication and Improved Lithography by Directed Block Copolymer Assembly," *Science,* vol. 321, no. 5891, p. 936, **2008**.

[79] L. Chi-Chun, P. F. Nealey, A. K. Raub, P. J. Hakeem, S. R. J. Brueck, H. Eungnak, and P. Gopalan, "Integration of block copolymer directed assembly with 193 immersion lithography," *Journal of Vacuum Science & Technology B (Microelectronics and Nanometer Structures),* vol. 28, no. 6, pp. C6B30-C6B34, **2010**.

[80] J. Y. Cheng, A. M. Mayes, and C. A. Ross, "Nanostructure engineering by templated self-assembly of block copolymers," *Nature Materials,* vol. 3, no. 11, pp. 823-828, **2004**.

[81] D. Borah, S. Rassapa, M. T. Shaw, R. G. Hobbs, N. Petkov, M. Schmidt, J. D. Holmes, and M. A. Morris, "Directed self-assembly of PS-b-PMMA block

copolymer using HSQ lines for translational alignment," *Journal of Materials Chemistry C,* vol. 1, no. 6, pp. 1192-1196, **2013**.

[82] A. P. Lane, X. Yang, M. J. Maher, G. Blachut, Y. Asano, Y. Someya, A. Mallavarapu, S. M. Sirard, C. J. Ellison, and C. G. Willson, "Directed Self-Assembly and Pattern Transfer of Five Nanometer Block Copolymer Lamellae," *ACS Nano,* vol. 11, no. 8, pp. 7656-7665, **2017**.

[83] C. Chi, C.-C. Liu, L. Meli, K. Schmidt, Y. Xu, E. A. DeSilva, M. Sanchez, R. Farrell, H. Cottle, D. Kawamura, L. Singh, T. Furukawa, K. Lai, J. W. Pitera, D. Sanders, D. R. Hetzer, A. Metz, N. Felix, J. Arnold, and M. Colburn, "DSA via hole shrink for advanced node applications," in *SPIE Advanced Lithography*, 2016, vol. 9777: SPIE, p. 97770L.

[84] J. G. Son, W. K. Bae, H. Kang, P. F. Nealey, and K. Char, "Placement Control of Nanomaterial Arrays on the Surface-Reconstructed Block Copolymer Thin Films," *ACS Nano,* vol. 3, no. 12, pp. 3927-3934, **2009**.

[85] D. F. Sunday, E. Ashley, L. Wan, K. C. Patel, R. Ruiz, and R. J. Kline, "Template–polymer commensurability and directed self-assembly block copolymer lithography," *Journal of Polymer Science Part B: Polymer Physics,* vol. 53, no. 8, pp. 595-603, **2015**.

[86] E. Verploegen, L. C. McAfee, L. Tian, D. Verploegen, and P. T. Hammond, "Observation of Transverse Cylinder Morphology in Side Chain Liquid Crystalline Block Copolymers," *Macromolecules,* vol. 40, no. 4, pp. 777-780, **2007**.

[87] B. C. Berry, A. W. Bosse, J. F. Douglas, R. L. Jones, and A. Karim, "Orientational Order in Block Copolymer Films Zone Annealed below the Order−Disorder Transition Temperature," *Nano Letters,* vol. 7, no. 9, pp. 2789-2794, **2007**.

[88] C. Tang, A. Tracz, M. Kruk, R. Zhang, D.-M. Smilgies, K. Matyjaszewski, and T. Kowalewski, "Long-Range Ordered Thin Films of Block Copolymers Prepared by Zone-Casting and Their Thermal Conversion into Ordered Nanostructured Carbon," *Journal of the American Chemical Society,* vol. 127, no. 19, pp. 6918-6919, **2005**.

[89] C. Liedel, C. W. Pester, M. Ruppel, C. Lewin, M. J. Pavan, V. S. Urban, R. Shenhar, P. Bösecke, and A. Böker, "Block Copolymer Nanocomposites in Electric Fields: Kinetics of Alignment," *ACS Macro Letters,* vol. 2, no. 1, pp. 53-58, **2013**.

[90] P. W. Majewski, M. Gopinadhan, W. S. Jang, J. L. Lutkenhaus, and C. O. Osuji, "Anisotropic ionic conductivity in block copolymer membranes by magnetic field alignment," *J Am Chem Soc,* vol. 132, no. 49, pp. 17516-22, **2010**.

[91] D. Wu, F. Xu, B. Sun, R. Fu, H. He, and K. Matyjaszewski, "Design and Preparation of Porous Polymers," *Chemical Reviews,* vol. 112, no. 7, pp. 3959-4015, **2012**.

[92] Z. Cui and SpringerLink, *Nanofabrication. Principles, Capabilities and Limits*, 2nd ed. 2017. ed. Springer International Publishing, **2017**.

[93] L. Shuai, W. Lihua, L. Biqian, and S. Yanlin, "pH responsiveness of two-layer nano-composite membrane with ultrathin cylindrical nanopores PS-b-P4VP film," *Polymer,* vol. 54, no. 12, pp. 3065-3070, **2013**.

[94] T. Thurn-Albrecht, R. Steiner, J. DeRouchey, C. M. Stafford, E. Huang, M. Bal, M. Tuominen, C. J. Hawker, and T. P. Russell, "Nanoscopic Templates from Oriented Block Copolymer Films," *Advanced Materials,* vol. 12, no. 11, pp. 787-791, **2000**.

[95] Y.-H. Ting, S.-M. Park, C.-C. Liu, X. Liu, F. J. Himpsel, P. F. Nealey, and A. E. Wendt, "Plasma etch removal of poly(methyl methacrylate) in block copolymer lithography," *Journal of Vacuum Science & Technology B: Microelectronics and Nanometer Structures Processing, Measurement, and Phenomena,* vol. 26, no. 5, pp. 1684-1689, **2008**.

[96] J. Chai and J. M. Buriak, "Using Cylindrical Domains of Block Copolymers To Self-Assemble and Align Metallic Nanowires," *ACS Nano,* vol. 2, no. 3, pp. 489-501, **2008**.

[97] B.-H. Sohn, S.-I. Yoo, B.-W. Seo, S.-H. Yun, and S.-M. Park, "Nanopatterns by Free-Standing Monolayer Films of Diblock Copolymer Micelles with in Situ Core−Corona Inversion," *Journal of the American Chemical Society,* vol. 123, no. 50, pp. 12734-12735, **2001**.

[98] S. Park, J.-Y. Wang, B. Kim, and T. P. Russell, "From Nanorings to Nanodots by Patterning with Block Copolymers," *Nano Letters,* vol. 8, no. 6, pp. 1667-1672, **2008**.

[99] C. Xu, X. Fu, M. Fryd, S. Xu, B. B. Wayland, K. I. Winey, and R. J. Composto, "Reversible Stimuli-Responsive Nanostructures Assembled from Amphiphilic Block Copolymers," *Nano Letters,* vol. 6, no. 2, pp. 282-287, **2006**.

[100] T. Xu, J. T. Goldbach, M. J. Misner, S. Kim, A. Gibaud, O. Gang, B. Ocko, K. W. Guarini, C. T. Black, C. J. Hawker, and T. P. Russell, "Scattering Study on the Selective Solvent Swelling Induced Surface Reconstruction," *Macromolecules,* vol. 37, no. 8, pp. 2972-2977, **2004**.

[101] K. Shin and J. Bae, "Nanoporous carbon template from surface reconstruction in block copolymer thin film," *Thin Solid Films,* vol. 520, no. 6, pp. 2351-2355, **2012**.

[102] S. Park, J.-Y. Wang, B. Kim, J. Xu, and T. P. Russell, "A Simple Route to Highly Oriented and Ordered Nanoporous Block Copolymer Templates," *ACS Nano,* vol. 2, no. 4, pp. 766-772, **2008**.

[103] C. Cummins, D. Borah, S. Rasappa, A. Chaudhari, T. Ghoshal, B. M. D. O'Driscoll, P. Carolan, N. Petkov, J. D. Holmes, and M. A. Morris, "Self-assembly of polystyrene-block-poly(4-vinylpyridine) block copolymer on molecularly functionalized silicon substrates: fabrication of inorganic nanostructured etchmask for lithographic use," *Journal of Materials Chemistry C,* vol. 1, no. 47, pp. 7941-7951, **2013**.

[104] H. Cho, H. Park, T. P. Russell, and S. Park, "Precise placements of metal nanoparticles from reversible block copolymer nanostructures," *Journal of Materials Chemistry,* vol. 20, no. 24, pp. 5047-5051, **2010**.

[105] L. Wang, F. Montagne, P. Hoffmann, and R. Pugin, "Gold nanoring arrays from responsive block copolymer templates," *Chemical Communications,* no. 25, pp. 3798-3800, **2009**.

[106] E. B. Gowd, B. Nandan, M. K. Vyas, N. C. Bigall, A. Eychmuller, H. Schlorb, and M. Stamm, "Highly ordered palladium nanodots and nanowires from switchable block copolymer thin films," *Nanotechnology,* vol. 20, no. 41, p. 415302, **2009**.

[107] G. P. Gakis, H. Vergnes, E. Scheid, C. Vahlas, A. G. Boudouvis, and B. Caussat, "Detailed investigation of the surface mechanisms and their interplay with transport phenomena in alumina atomic layer deposition from TMA and water," *Chemical Engineering Science,* vol. 195, pp. 399-412, **2019**.

[108] F. Yang, J. Brede, H. Ablat, M. Abadia, L. Zhang, C. Rogero, S. D. Elliott, and M. Knez, "Reversible and Irreversible Reactions of Trimethylaluminum with Common Organic Functional Groups as a Model for Molecular Layer Deposition and Vapor Phase Infiltration," *Advanced Materials Interfaces,* vol. 4, no. 18, p. 1700237, **2017**.

[109] Q. Peng, Y.-C. Tseng, S. B. Darling, and J. W. Elam, "A Route to Nanoscopic Materials via Sequential Infiltration Synthesis on Block Copolymer Templates," *ACS Nano,* vol. 5, no. 6, pp. 4600-4606, **2011**.

[110] R. Z. Waldman, D. J. Mandia, A. Yanguas-Gil, A. B. F. Martinson, J. W. Elam, and S. B. Darling, "The chemical physics of sequential infiltration synthesis—A thermodynamic and kinetic perspective," *The Journal of Chemical Physics,* vol. 151, no. 19, p. 190901, **2019**.

[111] B. Gong and G. N. Parsons, "Quantitative in situ infrared analysis of reactions between trimethylaluminum and polymers during Al2O3 atomic layer deposition," *Journal of Materials Chemistry,* vol. 22, no. 31, pp. 15672-15682, **2012**.

[112] K.-H. Shen, J. R. Brown, and L. M. Hall, "Diffusion in Lamellae, Cylinders, and Double Gyroid Block Copolymer Nanostructures," *ACS Macro Letters,* vol. 7, no. 9, pp. 1092-1098, **2018**.

[113] I. Weisbord, N. Shomrat, R. Azoulay, A. Kaushansky, and T. Segal-Peretz, "Understanding and Controlling Polymer–Organometallic Precursor Interactions in Sequential Infiltration Synthesis," *Chemistry of Materials,* vol. 32, no. 11, pp. 4499-4508, **2020**.

[114] Q. Peng, Y.-C. Tseng, S. B. Darling, and J. W. Elam, "Nanoscopic Patterned Materials with Tunable Dimensions via Atomic Layer Deposition on Block Copolymers," *Advanced Materials,* vol. 22, no. 45, pp. 5129-5133, **2010**.

[115] E. C. Dandley, C. D. Needham, P. S. Williams, A. H. Brozena, C. J. Oldham, and G. N. Parsons, "Temperature-dependent reaction between trimethylaluminum and poly(methyl methacrylate) during sequential vapor infiltration: experimental and ab initio analysis," *Journal of Materials Chemistry C,* vol. 2, no. 44, pp. 9416-9424, **2014**.

[116] M. Biswas, J. A. Libera, S. B. Darling, and J. W. Elam, "New Insight into the Mechanism of Sequential InfiltrationSynthesis from Infrared Spectroscopy," *Chemistry of Materials,* vol. 26, no. 21, pp. 6135-6141, **2014**.

[117] M. Snelgrove, C. McFeely, K. Shiel, G. Hughes, P. Yadav, C. Weiland, J. C. Woicik, P. G. Mani-Gonzalez, R. Lundy, M. A. Morris, E. McGlynn, and R. O'Connor, "Analysing trimethylaluminum infiltration into polymer brushes using a scalable area selective vapor phase process," *Materials Advances,* vol. 2, no. 2, pp. 769-781, **2021**.

[118] D. H. Yi, C.-Y. Nam, G. Doerk, C. T. Black, and R. B. Grubbs, "Infiltration Synthesis of Diverse Metal Oxide Nanostructures from Epoxidized Diene–Styrene Block Copolymer Templates," *ACS Applied Polymer Materials,* vol. 1, no. 4, pp. 672-683, **2019**.

[119] G. T. Hill, D. T. Lee, P. S. Williams, C. D. Needham, E. C. Dandley, C. J. Oldham, and G. N. Parsons, "Insight on the Sequential Vapor Infiltration Mechanisms of Trimethylaluminum with Poly(methyl methacrylate), Poly(vinylpyrrolidone), and Poly(acrylic acid)," *The Journal of Physical Chemistry C,* vol. 123, no. 26, pp. 16146-16152, **2019**.

[120] G. Kästle, H. G. Boyen, F. Weigl, G. Lengl, T. Herzog, P. Ziemann, S. Riethmüller, O. Mayer, C. Hartmann, J. P. Spatz, M. Möller, M. Ozawa, F. Banhart, M. G. Garnier, and P. Oelhafen, "Micellar Nanoreactors—Preparation and Characterization of Hexagonally Ordered Arrays of Metallic Nanodots," *Advanced Functional Materials,* vol. 13, no. 11, pp. 853-861, **2003**.

[121] K. R. Williams, K. Gupta, and M. Wasilik, "Etch rates for micromachining processing-Part II," *Journal of Microelectromechanical Systems,* vol. 12, no. 6, pp. 761-778, **2003**.

[122] P. Naulleau, "2.17 - Optical Lithography," in *Comprehensive Nanoscience and Nanotechnology (Second Edition)*, D. L. Andrews, R. H. Lipson, and T. Nann Eds. Oxford: Academic Press, **2019**, pp. 387-398.

[123] J. Albero, L. Nieradko, C. Gorecki, H. Ottevaere, V. Gomez, H. Thienpont, J. Pietarinen, B. Päivänranta, and N. Passilly, "Fabrication of spherical microlenses by a combination of isotropic wet etching of silicon and molding techniques," *Opt. Express,* vol. 17, no. 8, pp. 6283-6292, **2009**.

[124] J. J. Kelly and H. G. G. Philipsen, "Anisotropy in the wet-etching of semiconductors," *Current Opinion in Solid State and Materials Science,* vol. 9, no. 1, pp. 84-90, **2005**.

[125] H. Lu, H. Zhang, M. Jin, T. He, G. Zhou, and L. Shui, "Two-Layer Microstructures Fabricated by One-Step Anisotropic Wet Etching of Si in KOH Solution," *Micromachines,* vol. 7, no. 2, **2016**.

[126] M. Huff, "Recent Advances in Reactive Ion Etching and Applications of High-Aspect-Ratio Microfabrication," *Micromachines,* vol. 12, no. 8, **2021**.

[127] P. Kaspar, Y. Jeyaram, H. Jäckel, A. Foelske, R. Kötz, and S. Bellini, "Silicon nitride hardmask fabrication using a cyclic CHF3-based reactive ion etching process for vertical profile nanostructures," *Journal of Vacuum Science & Technology B,* vol. 28, no. 6, pp. 1179-1186, **2010**.

[128] S. Aachboun, P. Ranson, C. Hilbert, and M. Boufnichel, "Cryogenic etching of deep narrow trenches in silicon," *Journal of Vacuum Science & Technology A,* vol. 18, no. 4, pp. 1848-1852, **2000**.

[129] X. Gu, Z. Liu, I. Gunkel, S. T. Chourou, S. W. Hong, D. L. Olynick, and T. P. Russell, "High Aspect Ratio Sub-15 nm Silicon Trenches From Block Copolymer Templates," *Advanced Materials,* vol. 24, no. 42, pp. 5688-5694, **2012**.

[130] A. J. Hong, C.-C. Liu, Y. Wang, J. Kim, F. Xiu, S. Ji, J. Zou, P. F. Nealey, and K. L. Wang, "Metal Nanodot Memory by Self-Assembled Block Copolymer Lift-Off," *Nano Letters,* vol. 10, no. 1, pp. 224-229, **2010**.

[131] Z. Honggang, Z. Nan, M. Gilchrist, and F. Fengzhou, "Advances in precision micro/nano-electroforming: a state-of-the-art review," *Journal of Micromechanics and Microengineering,* vol. 30, no. 10, p. 103002, **2020**.

[132] R. Jafari Jam, M. Heurlin, V. Jain, A. Kvennefors, M. Graczyk, I. Maximov, M. T. Borgström, H. Pettersson, and L. Samuelson, "III–V Nanowire Synthesis by Use of Electrodeposited Gold Particles," *Nano Letters,* vol. 15, no. 1, pp. 134-138, **2015**.

[133] H. Komiyama, "Fabrication of a Vertically Aligned Au Nanorod Array via Block-Copolymer-Templated Electroplating," *ChemistrySelect,* vol. 3, no. 17, pp. 4944-4950, **2018**.

[134] F. H. Jin, W. Peter, and Z. Margit, "Semiconductor Nanowires: From Self-Organization to Patterned Growth," *Small,* vol. 2, no. 6, pp. 700-717, **2006**.

[135] L. Samuelson, "Self-forming nanoscale devices," *Materials Today,* vol. 6, no. 10, pp. 22-31, **2003**.

[136] K. Tomioka, K. Ikejiri, T. Tanaka, J. Motohisa, S. Hara, K. Hiruma, and T. Fukui, "Selective-area growth of III-V nanowires and their applications," *Journal of Materials Research,* vol. 26, no. 17, pp. 2127-2141, **2011**.

[137] K. Tomioka, P. Mohan, J. Noborisaka, S. Hara, J. Motohisa, and T. Fukui, "Growth of highly uniform InAs nanowire arrays by selective-area MOVPE," *Journal of Crystal Growth,* vol. 298, pp. 644-647, **2007**.

[138] K. Tomioka, T. Tanaka, S. Hara, K. Hiruma, and T. Fukui, "III–V Nanowires on Si Substrate: Selective-Area Growth and Device Applications," *IEEE Journal of Selected Topics in Quantum Electronics,* vol. 17, no. 4, pp. 1112-1129, **2011**.

[139] I. Yang, X. Zhang, C. Zheng, Q. Gao, Z. Li, L. Li, M. N. Lockrey, H. Nguyen, P. Caroff, J. Etheridge, H. H. Tan, C. Jagadish, J. Wong-Leung, and L. Fu, "Radial Growth Evolution of InGaAs/InP Multi-Quantum-Well Nanowires Grown by Selective-Area Metal Organic Vapor-Phase Epitaxy," *ACS Nano,* vol. 12, no. 10, pp. 10374-10382, **2018**.

[140] J. Na, S. Lee, and S. Lim, "Oxidation and etching behaviors of the InAs surface in various acidic and basic chemical solutions," *Surface Science,* vol. 658, pp. 22-30, **2017**.

[141] S. T. Šuran Brunelli, A. Goswami, B. Markman, H.-Y. Tseng, M. Rodwell, C. Palmstrøm, and J. Klamkin, "Horizontal Heterojunction Integration via Template-Assisted Selective Epitaxy," *Crystal Growth & Design,* vol. 19, no. 12, pp. 7030-7035, **2019**.

[142] J. K. Hyun, S. Zhang, and L. J. Lauhon, "Nanowire Heterostructures," *Annual Review of Materials Research,* vol. 43, no. 1, pp. 451-479, **2013**.

[143] K. Tomioka, J. Motohisa, S. Hara, and T. Fukui, "Crystallographic Structure of InAs Nanowires Studied by Transmission Electron Microscopy," *Japanese Journal of Applied Physics,* vol. 46, no. No. 45, pp. L1102-L1104, **2007**.

[144] O.-P. Kilpi, J. Svensson, J. Wu, A. R. Persson, R. Wallenberg, E. Lind, and L.-E. Wernersson, "Vertical InAs/InGaAs Heterostructure Metal–Oxide–Semiconductor Field-Effect Transistors on Si," *Nano Letters,* vol. 17, no. 10, pp. 6006-6010, **2017**.

[145] T. Vasen, P. Ramvall, A. Afzalian, G. Doornbos, M. Holland, C. Thelander, K. A. Dick, L. E. Wernersson, and M. Passlack, "Vertical Gate-All-Around Nanowire GaSb-InAs Core-Shell n-Type Tunnel FETs," *Scientific Reports,* vol. 9, no. 1, p. 202, **2019**.

[146] K. A. Dick, K. Deppert, L. Samuelson, and W. Seifert, "InAs nanowires grown by MOVPE," *Journal of Crystal Growth,* vol. 298, pp. 631-634, **2007**.

[147] L. J. Mawst, J. H. Park, A. A. Khandekar, S. M. Park, T. F. Kuech, and P. F. Nealey, "Selective MOCVD growth of single-crystal dense GaAs quantum dot array using cylinder-forming diblock copolymers," *Journal of Crystal Growth,* vol. 297, no. 2, pp. 283-8, **2006**.

[148] J. H. Park, J. Kirch, L. J. Mawst, C.-C. Liu, P. F. Nealey, and T. F. Kuech, "Controlled growth of InGaAs/InGaAsP quantum dots on InP substrates employing diblock copolymer lithography," *Applied Physics Letters,* vol. 95, no. 11, p. 113111, **2009**.

[149] T. F. Kuech and L. J. Mawst, "Nanofabrication of III-V semiconductors employing diblock copolymer lithography," *Journal of Physics D: Applied Physics,* vol. 43, no. 18, p. 183001 (18 pp.), **2010**.

[150] H. Kim, J. Choi, Z. Lingley, M. Brodie, Y. Sin, T. F. Kuech, P. Gopalan, and L. J. Mawst, "Selective growth of strained (In)GaAs quantum dots on GaAs substrates employing diblock copolymer lithography nanopatterning," *Journal of Crystal Growth,* vol. 465, pp. 48-54, **2017**.

[151] Y. Huang, T. W. Kim, S. Xiong, L. J. Mawst, T. F. Kuech, P. F. Nealey, Y. Dai, Z. Wang, W. Guo, D. Forbes, S. M. Hubbard, and M. Nesnidal, "InAs Nanowires Grown by Metal–Organic Vapor-Phase Epitaxy (MOVPE) Employing PS/PMMA Diblock Copolymer Nanopatterning," *Nano Letters,* vol. 13, no. 12, pp. 5979-5984, **2013**.

[152] W. Ogieglo, H. Wormeester, K.-J. Eichhorn, M. Wessling, and N. E. Benes, "In situ ellipsometry studies on swelling of thin polymer films: A review," *Progress in Polymer Science,* vol. 42, pp. 42-78, **2015**.

[153] E. A. Irene, "A Brief History and State of the Art of Ellipsometry," in *Ellipsometry at the Nanoscale*, M. Losurdo and K. Hingerl Eds. Berlin, Heidelberg: Springer Berlin Heidelberg, **2013**, pp. 1-30.

[154] E. Cianci, D. Nazzari, G. Seguini, and M. Perego, "Trimethylaluminum Diffusion in PMMA Thin Films during Sequential Infiltration Synthesis: In Situ Dynamic Spectroscopic Ellipsometric Investigation," *Advanced Materials Interfaces,* vol. 5, no. 20, p. 1801016, **2018**.

[155] J. W. Elam, M. Biswas, S. B. Darling, A. Yanguas-Gil, J. D. Emery, A. B. F. Martinson, P. F. Nealey, T. Segal-Peretz, Q. Peng, J. Winterstein, J. A. Liddle, and Y.-C. Tseng, "New Insights into Sequential Infiltration Synthesis," *ECS Trans,* vol. 69, no. 7, pp. 147-157, **2015**.

[156] F. Gramazio, M. Lorenzoni, F. Pérez-Murano, L. Evangelio, and J. Fraxedas, "Quantification of nanomechanical properties of surfaces by higher harmonic

monitoring in amplitude modulated AFM imaging," *Ultramicroscopy,* vol. 187, pp. 20-25, **2018**.

[157] H. Ott, V. Abetz, V. Altstadt, Y. Thomann, and A. Pfau, "Comparative study of a block copolymer morphology by transmission electron microscopy and scanning force microscopy," *Journal of Microscopy,* vol. 205, pp. 106-108, **2002**.

[158] A. Ul-Hamid, *A Beginners' Guide to Scanning Electron Microscopy*. Springer, **2018**.

[159] T. Segal-Peretz, J. Winterstein, M. Doxastakis, A. Ramírez-Hernández, M. Biswas, J. Ren, H. S. Suh, S. B. Darling, J. A. Liddle, J. W. Elam, J. J. de Pablo, N. J. Zaluzec, and P. F. Nealey, "Characterizing the Three-Dimensional Structure of Block Copolymers via Sequential Infiltration Synthesis and Scanning Transmission Electron Tomography," *ACS Nano,* vol. 9, no. 5, pp. 5333-5347, **2015**.

[160] P. Müller-Buschbaum, "GISAXS and GISANS as metrology technique for understanding the 3D morphology of block copolymer thin films," *European Polymer Journal,* vol. 81, pp. 470-493, **2016**.

[161] N. Torikai, N. L. Yamada, A. Noro, M. Harada, D. Kawaguchi, A. Takano, and Y. Matsushita, "Neutron Reflectometry on Interfacial Structures of the Thin Films of Polymer and Lipid," *Polymer Journal,* vol. 39, p. 1238, **2007**.

[162] N. Torikai, A. Noro, M. Okuda, F. Odamaki, D. Kawaguchi, A. Takano, and Y. Matsushita, "Neutron Reflection Studies on Lamellar Microphase-Separated Structures of Two-Component Block Copolymers with Composition Distribution," *Physica B: Physics of Condensed Matter,* vol. 385, no. Part 1, pp. 709-712, **2006**.

[163] V. F. Sears, "Neutron scattering lengths and cross sections," *Neutron News,* vol. 3, no. 3, pp. 26-37, **1992**.

[164] A. Vorobiev, A. Devishvilli, G. Palsson, H. Rundlöf, N. Johansson, A. Olsson, A. Dennison, M. Wollf, B. Giroud, O. Aguettaz, and B. Hjörvarsson, "Recent upgrade of the polarized neutron reflectometer Super ADAM," *Neutron News,* vol. 26, no. 3, pp. 25-26, **2015**.

[165] A. Devishvili, K. Zhernenkov, A. J. C. Dennison, B. P. Toperverg, M. Wolff, B. Hjörvarsson, and H. Zabel, "SuperADAM: Upgraded polarized neutron reflectometer at the Institut Laue-Langevin," *Review of Scientific Instruments,* vol. 84, no. 2, p. 025112, **2013**.

[166] R. A. Campbell, "Recent advances in resolving kinetic and dynamic processes at the air/water interface using specular neutron reflectometry," *Current Opinion in Colloid & Interface Science,* vol. 37, pp. 49-60, **2018**.

[167] M. Berg, O.-P. Kilpi, K.-M. Persson, J. Svensson, M. Hellenbrand, E. Lind, and L.-E. Wernersson, "Electrical Characterization and Modeling of Gate-Last

Vertical InAs Nanowire MOSFETs on Si," *IEEE Electron Device Letters,* vol. 37, no. 8, p. 966, **2016**.

[168] A. Fontcuberta i Morral, "Gold-Free GaAs Nanowire Synthesis and Optical Properties," *IEEE Journal of Selected Topics in Quantum Electronics, Selected Topics in Quantum Electronics, IEEE Journal of, IEEE J. Select. Topics Quantum Electron.,* no. 4, p. 819, **2011**.

[169] V. Dagyte, E. Barrigon, W. Zhang, X. Zeng, M. Heurlin, G. Otnes, N. Anttu, and M. T. Borgstrom, "Time-resolved photoluminescence characterization of GaAs nanowire arrays on native substrate," vol. 28, ed, **2017**.

[170] J. H. Shin, H. G. Kim, G. M. Baek, R. Kim, S. Jeon, J. H. Mun, H.-B.-R. Lee, Y. S. Jung, S. O. Kim, K. N. Kim, and G. Y. Yeom, "Fabrication of 50 nm scale Pt nanostructures by block copolymer (BCP) and its characteristics of surface-enhanced Raman scattering (SERS)," *RSC Advances,* vol. 6, no. 75, pp. 70756-70762, **2016**.

[171] O. Hellwig, J. K. Bosworth, E. Dobisz, D. Kercher, T. Hauet, G. Zeltzer, J. D. Risner-Jamtgaard, D. Yaney, and R. Ruiz, "Bit patterned media based on block copolymer directed assembly with narrow magnetic switching field distribution," *Applied Physics Letters,* vol. 96, no. 5, p. 052511, **2010**.

[172] E. Memisevic, J. Svensson, E. Lind, and L. Wernersson, "Vertical Nanowire TFETs With Channel Diameter Down to 10 nm and Point SMIN of 35 mV/Decade," *IEEE Electron Device Letters,* vol. 39, no. 7, pp. 1089-1091, **2018**.

[173] V. Pelletier, K. Asakawa, W. Mingshaw, D. H. Adamson, R. A. Register, and P. M. Chaikin, "Aluminum nanowire polarizing grids: fabrication and analysis," *Applied Physics Letters,* vol. 88, no. 21, pp. 211114-1-3, **2006**.

[174] C. Yu-Cheng, I. Otsuka, S. Halila, R. Borsali, and C. Wen-Chang, "High-performance nonvolatile transistor memories of pentacence using the green electrets of sugar-based block copolymers and their supramolecules," *Advanced Functional Materials,* vol. 24, no. 27, pp. 4240-4249, **2014**.

[175] S. Rasappa, D. Borah, C. C. Faulkner, T. Lutz, M. T. Shaw, J. D. Holmes, and M. A. Morris, "Fabrication of a Sub-10 nm silicon nanowire based ethanol sensor using block copolymer lithography," *Nanotechnology,* vol. 24, no. 6, p. 065503, **2013**.

[176] T. Yu-Chih and S. B. Darling, "Block Copolymer Nanostructures for Technology," *Polymers (20734360),* vol. 2, no. 4, pp. 470-489, **2010**.

[177] S. H. Kim, J.-D. Park, and K.-D. Lee, "Fabrication of a nano-wire grid polarizer for brightness enhancement in liquid crystal display," *Nanotechnology,* vol. 17, no. 17, pp. 4436-4438, **2006**.

[178] "International Roadmap for Devices and Systems, Emerging Reseach Materials." IEEE. https://irds.ieee.org/editions/2017/emerging-research-materials (accessed 23 September 2021).

[179] M. Graczyk, A. Cattoni, B. Rosner, G. Seniutinas, A. Lofstrand, A. Kvennefors, D. Mailly, C. David, and I. Maximov, "Nanoimprint stamps with ultra-high resolution: Optimal fabrication techniques," *Microelectronic Engineering,* vol. 190, pp. 73-78, **2018**.

[180] S. Y. Yang, I. Ryu, H. Y. Kim, J. K. Kim, S. K. Jang, and T. P. Russell, "Nanoporous Membranes with Ultrahigh Selectivity and Flux for the Filtration of Viruses," *Advanced Materials,* vol. 18, no. 6, pp. 709-712, **2006**.

[181] M. Radjabian and V. Abetz, "Advanced porous polymer membranes from self-assembling block copolymers," *Progress in Polymer Science,* vol. 102, p. 101219, **2020**.

[182] P. S. Jo, Y. J. Park, S. J. Kang, T. H. Kim, C. Park, E. Kim, D. Y. Ryu, and H.-C. Kim, "Self assembled block copolymer gate insulators with cylindrical nanostructures for pentacene thin film transistor," *Macromolecular Research,* vol. 18, no. 8, pp. 777-786, **2010**.

[183] I. Otsuka, N. Nilsson, D. B. Suyatin, I. Maximov, and R. Borsali, "Carbohydrate-based block copolymer systems: directed self-assembly for nanolithography applications," *Soft Matter,* vol. 13, no. 40, pp. 7406-7411, **2017**.

[184] E. Lind and L. Wernersson, "Design of RF Properties for Vertical Nanowire MOSFETs," *IEEE Transactions on Nanotechnology,* vol. 10, no. 4, pp. 668-673, **2011**.

[185] E. Memišević, J. Svensson, M. Hellenbrand, E. Lind, and L. Wernersson, "Scaling of Vertical InAs–GaSb Nanowire Tunneling Field-Effect Transistors on Si," *IEEE Electron Device Letters,* vol. 37, no. 5, pp. 549-552, **2016**.

[186] A. C. Ford, J. C. Ho, Y.-L. Chueh, Y.-C. Tseng, Z. Fan, J. Guo, J. Bokor, and A. Javey, "Diameter-Dependent Electron Mobility of InAs Nanowires," *Nano Letters,* vol. 9, no. 1, pp. 360-365, **2009**.

[187] L. Forbes, "Gold in silicon: Characterisation and infra-red detector applications," *Gold Bulletin,* vol. 10, pp. 49-53, **1977**.

[188] S. Liu, L. Wang, B. Liu, and Y. Song, "pH responsiveness of two-layer nano-composite membrane with ultrathin cylindrical nanopores PS-b-P4VP film," *Polymer,* vol. 54, no. 12, pp. 3065-3070, **2013**.

[189] C. Atul, G. Tandra, T. S. Matthew, C. Cian, B. Dipu, D. H. Justin, and A. M. Michael, "Formation of sub-7 nm feature size PS-b-P4VP block copolymer structures by solvent vapour process," in *SPIE Advanced Lithography*, 2014, vol. 9051: SPIE, **2014**, pp. 905510-1-905510-10.

[190] A. Veloso, E. Altamirano-Sanchez, S. Brus, B. T. Chan, M. Cupak, M. Dehan, C. Delvaux, K. Devriendt, G. Eneman, M. Ercken, T. Huynh-Bao, T. Ivanov, P. Matagne, C. Merckling, V. Paraschiv, S. Ramesh, E. Rosseel, L. Rynders, A. Sibaja-Hernandez, S. Suhard, Z. Tao, E. Vecchio, N. Waldron, D. Yakimets, K. De Meyer, D. Mocuta, N. Collaert, and A. Thean, "(Invited) Vertical Nanowire FET Integration and Device Aspects," *ECS Trans,* vol. 72, no. 4, pp. 31-42, **2016**.

[191] F. Lindelöw, N. Sri Garigapati, L. Södergren, M. Borg, and E. Lind, "III–V nanowire MOSFETs with novel self-limiting Λ-ridge spacers for RF applications," *Semiconductor Science and Technology,* vol. 35, no. 6, p. 065015, **2020**.

[192] Z. Yong, K.-M. Persson, M. Saketh Ram, G. D'Acunto, Y. Liu, S. Benter, J. Pan, Z. Li, M. Borg, A. Mikkelsen, L.-E. Wernersson, and R. Timm, "Tuning oxygen vacancies and resistive switching properties in ultra-thin HfO2 RRAM via TiN bottom electrode and interface engineering," *Applied Surface Science,* vol. 551, p. 149386, **2021**.

[193] A. Jönsson, J. Svensson, and L. Wernersson, "A Self-Aligned Gate-Last Process Applied to All-III–V CMOS on Si," *IEEE Electron Device Letters,* vol. 39, no. 7, pp. 935-938, **2018**.

[194] L. Jiajing, A. R.-D. Paulina, S. Hyo Seon, M. Geert, and F. N. Paul, "Kinetic approach to defect reduction in directed self-assembly," *Journal of Micro/Nanolithography, MEMS, and MOEMS,* vol. 18, no. 4, pp. 1-7, **2019**.

[195] S. D. Brotherton, J. R. Ayres, A. Gill, H. W. van Kesteren, and F. J. A. M. Greidanus, "Deep levels of copper in silicon," *Journal of Applied Physics,* vol. 62, no. 5, pp. 1826-1832, **1987**.

[196] P.-M. Coulon, B. Damilano, B. Alloing, P. Chausse, S. Walde, J. Enslin, R. Armstrong, S. Vézian, S. Hagedorn, T. Wernicke, J. Massies, J. Zúñiga-Pérez, M. Weyers, M. Kneissl, and P. A. Shields, "Displacement Talbot lithography for nano-engineering of III-nitride materials," *Microsystems & Nanoengineering,* vol. 5, no. 1, p. 52, **2019**.

[197] F. A. Vollenbroek, E. J. Spiertz, and H. J. J. Kroon, "Profile modification of resist patterns in optical lithography," *Polymer Engineering & Science,* vol. 23, no. 17, pp. 925-930, **1983**.

[198] S. Rasappa, L. Schulte, D. Borah, H. Hulkkonen, S. Ndoni, T. Salminen, R. Senthamaraikanan, M. A. Morris, and T. Niemi, "Morphology evolution of PS-b-PDMS block copolymer and its hierarchical directed self-assembly on block copolymer templates," *Microelectronic Engineering,* vol. 192, pp. 1-7, **2018**.

[199] R. Z. Waldman, N. Jeon, D. J. Mandia, O. Heinonen, S. B. Darling, and A. B. F. Martinson, "Sequential Infiltration Synthesis of Electronic Materials: Group

13 Oxides via Metal Alkyl Precursors," *Chemistry of Materials,* vol. 31, no. 14, pp. 5274-5285, **2019**.

[200] A. Mayer, D. Blenskens, J. Rond, C. Steinberg, M. Papenheim, S. Wang, J. Zajadacz, K. Zimmer, and H.-C. Scheer, "Imprint strategy for directed self-assembly of block copolymers," *Microelectronic Engineering,* vol. 176, pp. 94-100, **2017**.

Printed by Media-Tryck, Lund 2021 NORDIC SWAN ECOLABEL 3041 0903

Anette Löfstrand has written this doctoral dissertation in the field of patterning at the nanometer scale. It includes creation of features in silicon of 5 nm width, at 12 nm periodicity, via infiltration of metal-organic molecules into carbohydrate-based block copolymer, and investigation thereof using neutron reflectometry. It also includes fabrication of vertical III-V nanowires at about 50 nm periodicity in specific configurations, using templates patterned by directed self-assembly of block copolymers on a silicon platform. A path for gate stack deposition for vertical gate all-around transistors was also demonstrated at this high nanowire density.

LUND UNIVERSITY

Lund University
Faculty of Engineering
Department of Physics
Division of Solid State Physics
ISBN 978-91-8039-044-6